

Accepted Manuscript

Characteristics, controls and geological models of hydrocarbon accumulation in the Carboniferous volcanic reservoirs of the Chunfeng Oilfield, Junggar Basin, northwestern China

Yong Wang, Renchao Yang, Mingshui Song, Nils Lenhardt, Xinzheng Wang, Xuecai Zhang, Shaochun Yang, Jun Wang, Haifang Cao

PII: S0264-8172(18)30153-3

DOI: [10.1016/j.marpetgeo.2018.04.001](https://doi.org/10.1016/j.marpetgeo.2018.04.001)

Reference: JMPG 3308

To appear in: *Marine and Petroleum Geology*

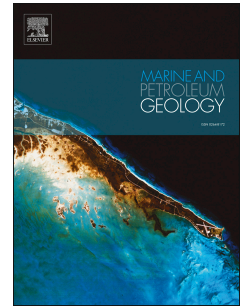
Received Date: 12 January 2018

Revised Date: 19 February 2018

Accepted Date: 1 April 2018

Please cite this article as: Wang, Y., Yang, R., Song, M., Lenhardt, N., Wang, X., Zhang, X., Yang, S., Wang, J., Cao, H., Characteristics, controls and geological models of hydrocarbon accumulation in the Carboniferous volcanic reservoirs of the Chunfeng Oilfield, Junggar Basin, northwestern China, *Marine and Petroleum Geology* (2018), doi: 10.1016/j.marpetgeo.2018.04.001.

This is a PDF file of an unedited manuscript that has been accepted for publication. As a service to our customers we are providing this early version of the manuscript. The manuscript will undergo copyediting, typesetting, and review of the resulting proof before it is published in its final form. Please note that during the production process errors may be discovered which could affect the content, and all legal disclaimers that apply to the journal pertain.



Characteristics, controls and geological models of hydrocarbon accumulation in the Carboniferous volcanic reservoirs of the Chunfeng Oilfield, Junggar Basin, northwestern China

Yong Wang^{1,2}, Renchao Yang^{3*}, Mingshui Song², Nils Lenhardt^{4*}, Xinzheng Wang²,
Xuecai Zhang², Shaochun Yang¹, Jun Wang², Haifang Cao²

¹School of Geosciences, China University of Petroleum, Qingdao, Shandong 266580, China

²Management Center of Oil and Gas Exploration, SINOPEC Shengli Oilfield Company, Dongying, Shandong 257001, China

³College of Earth Science and Technology, Shandong University of Science and Technology, Qingdao 266590, China

⁴Department of Geology, University of Pretoria, Private Bag X20, 0028 Pretoria, South Africa

*** Corresponding author**

Abstract:

The Junggar Basin is one of the most important basins for hydrocarbon production in China. Within the basin, the Chunfeng Oilfield forms one of the most important oilfields of the area. Despite the significant work that has been done on the rocks of the oilfield so far, a detailed reservoir characterization and description of the hydrocarbon accumulation pattern was still missing. Therefore, an investigation had been initiated to fill this gap in our understanding of the hydrocarbon reservoirs of the

Junggar Basin. The results of this study show that the tuff and andesitic lava lithofacies exhibit the highest reservoir potential in the area. Apart from the lithofacies, the results of this study show that tectonic (formation of fault systems) and diagenetic (formation of solution pores) effects, and the development of a weathering crust are crucial factors that control the quality of the petroleum reservoirs of the oilfield. In addition, two possible geological models of petroleum accumulation in isolated volcanic rocks and sandstone (IVRS) and connected volcanic rocks and sandstone (CVRS) are presented.

Keywords: Carboniferous; volcanic reservoir; reservoir properties; Junggar Basin; hydrocarbon accumulation

1. Introduction

With the global demand of hydrocarbons in the form of oil and gas for energy production constantly increasing while, at the same time, the reserves from conventional sources are getting depleted, unconventional resources are gaining increasingly higher importance. In recent years, volcanic or volcanic-derived rocks from a variety of basinal settings, representing approximately 1% of the world's total proven oil and gas reserves, have become a major target for hydrocarbon exploration (e.g., Zou et al., 2008; Zhao et al., 2009; Schutter, 2003a). Volcanic rock reservoirs are considered tight rock reservoirs as they are generally characterized by low porosities and permeabilities, a relatively small size, heterogenic lithology and burial depth in

the range of 400-2000 m (Feng, 2008). The rocks of these reservoirs may be related to effusive (lava) or explosive (tuff or ignimbrite at a variety of different degrees of welding) eruptions or the erosional product (tuffaceous sandstone, breccia, etc.) of these primary deposits. As volcanic and volcanoclastic rocks are more heterogeneous in their petrophysical properties than their (carbonate or siliciclastic) sedimentary counterparts, detailed studies on volcanic rock reservoirs are crucial to understand their complicated internal architecture (Levin, 1995; Sruoga et al., 2004; Lenhardt and Götz, 2011; Lenhardt and Götz, 2015).

Until now, oil and gas accumulations in volcanic rock reservoirs (including lava, primary volcanoclastic sediments and their erosional products) have been proven in more than 300 basins in 20 countries and regions (Schutter, 2003b). In many locations, such as Argentina (Sruoga et al., 2004; Sruoga and Rubinstein, 2007), Indonesia (Sembodo, 1973; Nayoan, 1981), Japan (Sakata, 1997; Magara, 2003), Russia (Levin, 1995), Venezuela (Landes et al., 1960) and China, hydrocarbon production from volcanic rock reservoirs is already in place. The most important basins for hydrocarbon production from volcanic reservoirs in China are the Junggar, Songliao, and Bohai Bay basins (e.g., Chen et al., 2016a; Qiu et al., 2016; Tang et al., 2016; Wei et al., 2017; Shi et al., 2017; Chen et al., 2017; Jiang et al., 2017; Luo et al., 2017). Due to its vast oil, natural gas, and coal resources, the Junggar Basin of western China, especially in recent years, has attained an immense economic significance (Tang et al., 1997; Chen et al., 2016a; Qiu et al., 2016; Shi et al., 2017; Chen et al., 2017). The Chunfeng Oilfield (CF Oilfield), located in the Chepaizi uplift at the northwestern

margin of the Junggar Basin, forms one of the most important oil yield of the area, with proven hydrocarbon reserves of $\sim 9.4 \times 10^8$ tons (Shengli Oilfield Company; personal communication).

The reservoir rocks of the CF Oilfield are predominantly characterized by volcanic and volcanoclastic rocks of Carboniferous age (Wu et al., 2014; Zhang and Yang, 2016). Previous studies in the area primarily focused on hydrocarbon sources (Zhang et al., 2014), reservoir properties (Wang et al., 2015), the weathering crust that developed on top of the volcanic rocks (Hou et al., 2013; Chen et al., 2016b), the tectonic evolution and fault formation mechanisms (Dong et al., 2015), and controlling factors for hydrocarbon accumulation (Hong et al., 2007; Li, 2013; Chen et al., 2016a). Nevertheless, due to the high variety in different lithologies and lithofacies, vertically and laterally variable formations, high heterogeneity, poor seismic reflections and changing oil-bearing potential, which had hindered the hydrocarbon exploration in the past (Song et al., 2007), not much information is available on the hydrocarbon accumulation pattern of the CF Oilfield. The aim of this contribution is therefore to 1) characterize the Carboniferous volcanic reservoir of the Chunfeng Oilfield, 2) discuss the hydrocarbon accumulation pattern in order to identify the hydrocarbon distribution, and 3) to provide reference for future exploration.

2. Geological setting

The Junggar Basin, a large intermontane superimposed basin, located in the Xinjiang

Uyghur Autonomous Region of Northwest China (Fig. 1A), covers a total area of 136,000 km², and is surrounded by mountains, i.e. the Zaire Mountains to the northwest, and the north Tianshan Mountains to the south (Song et al., 2007). Despite the fact that the surrounding mountain ranges are still active, the basin itself exhibits very little internal deformation. Instead, it records an exceptionally long history of subsidence and impoundment of sediments (Carroll et al., 2010). The CF Oilfield is located in the northeastern part of the Chepaizi Uplift at the northwestern margin of the Junggar Basin (Fig. 1B). The Hongche fault belt forms the boundary of the Chepaizi uplift to the Changji sag in the east. Furthermore, the Sikeshu sag is bordering the uplift to the south. The Piedmont Depression forms the southern boundary of the Junggar basin towards the Tianshan Mountains.

The Junggar Basin formed during the late Paleozoic to Middle Cenozoic as a result of the superimposition of a rift basin and a foreland basin (Wang and Yang, 2012). The tectonic evolution of the basin can be divided into four stages: (1) a cratonic inner and edge rifting stage (related to the Middle Hercynian Movement), (2) a peripheral foreland basin stage (Late Hercynian movement), (3) an intracontinental depression stage (Indosinian-Yanshanian movement), and (4) a para-foreland basin stage (Himalayan movement) (Zhang et al., 2014).

In the early Palaeozoic, the Junggar Basin was covered by the Paleo-Asian Ocean in a divergent regime. Subduction of the oceanic plate occurred in the Early Carboniferous, resulting in subduction-related volcanism during this period (Tao et al., 2006). In the late Carboniferous, the Junggar Basin was uplifted in the process of structural

compression due to collision of the combined Tarim–central Tian Shan Block with the northern Tianshan Block by post-collisional transcurrent tectonics (Li et al., 2008). As a result, deposition was interrupted for about 50 Ma, and an ancient weathering crust was formed on top of the Carboniferous volcanic rocks. Until the Early Permian, a rift basin developed and was characterized by deposition of shallow marine sandstones and mudstones, intercalated with thinly-bedded limestones and chert (Wang and Yang, 2012). The early Hercynian orogenic movement stopped the development of the rift basin and formed a regional angular unconformity between the Early and the Middle Permian (Li et al., 2008). During the Middle to Late Permian, a peripheral foreland basin developed, accompanied by a sedimentary facies shift from shallow marine to continental lacustrine. An intracontinental depression with lacustrine deposits developed from the Triassic to the Cretaceous, as a result of thrusts from the south, northwest and northeast in the Indosinian and the Yanshan orogenies (Wang and Yang, 2012). The lacustrine basin shrank due to basement uplift. Controlled by massive thrust of the Himalayan Orogeny, the Junggar Basin underwent a para-foreland basin stage with a ~7000 m accumulated thickness of sediments in the southwestern Changji Depression (Li et al., 2008). The strata of the Junggar Basin from Paleozoic to Cenozoic are sketched in Fig. 1D.

The Carboniferous strata involve three units (Li et al., 2015): (1) the lower volcanic unit followed by (2) a sedimentary unit and (3) the upper volcanic unit. The lower volcanic unit is dominated by andesite, dacite, rhyolite and tuff intercalated with minor basalt, whereas the upper volcanic unit is composed of basalt, andesite, rhyolite,

tuff with minor clastic sedimentary rocks. Zircon grains from the tuff in the lower volcanic unit are dated at 337.2 Ma using SHRIMP U–Pb method, and the middle sedimentary and upper volcanic units belong to Upper Carboniferous (Li et al., 2015). The burial depth of the Carboniferous volcanic reservoirs varies from 900 m in the northwestern part to >5000 m in the southeastern part (Fig. 1C). The maximum thickness encountered by drilling is about 2,000 m (not reach its bottom), and it may be larger than 5,000 m based on seismic interpretations. The Carboniferous rocks in the northwestern Junggar Basin include the Tailegula and Baogutu formations in the lower part and the Xibeikulasi Formation in the upper part (Fig. 2A). Drilling in the Carboniferous of the CF Oilfield revealed predominantly the Xibeikulasi Formation, which is the target in this study. In general, the Xibeikulasi Formation was deposited in a continental–neritic environment and is composed of a thick volcano-sedimentary sequence (Fig. 2B).

Source rocks of the Carboniferous volcanic rock reservoirs include the Permian, Jurassic and Cretaceous mudstone in adjacent Changji sag (Wang and Yang, 2012). Among them, the lacustrine Badaowan Formation (Jurassic) is regarded as the main source rocks of light crude in the Chepaizi uplift (Yuan et al., 2012). Cap rock (seals) are mainly the mudstone of the Paleogene Taxihe and Shawan formations, and the Cretaceous Tugulu Group (Wang and Yang, 2012; Yuan et al., 2012).

3. Materials and Methods

The results of this study are largely based on the PhD thesis of Wang (2018). In the

present contribution, however, only one representative seismic profile (dashed line in Fig. 1C) and a subsection of core data are included. Fault presence and locations within this contribution are based on interpretations of 3 seismic profiles. The weathering crusts of the seismic profiles and correlations were determined by integrated implementation of the information gained from drill cores, logging curves and the discontinuity of seismic coherent events.

Well logs of natural gamma-ray (GR), spontaneous potential (SP), acoustic (AC), shallow investigate double lateral resistivity (RS), deep investigate double lateral resistivity (RD), microsphere focused resistivity (MSFL), density (DEN), borehole diameter (CAL), compensated neutron log (CNL), fullbore formation microimager (FMI) from 57 wells (see Fig. 1C for locations) with interpretation of lithology and oil saturation by geophysical methods were obtained from the database of the Shengli Oilfield Company. Furthermore, porosity and permeability of the Carboniferous volcanic rocks of these 57 wells were calculated and interpreted based on multiple well logs (methodologies for calculation of porosity and permeability described in Hao et al., 2004). In addition, drill cores (25 runs) were collected from eight wells (well numbers CF51, CF59, CF60, CF69, CF70, CF71, CF73, and CF74; see Fig. 1C for locations) from the CF oilfield. The drill cores were examined and logged at scale 1:10. Finally, a total of 690 core samples were taken from the Carboniferous volcanic rocks. Of these 690 samples, 452 were used for thin sections (150 of these for stained thin sections, 50 for UV fluorescence thin sections, and 45 for scanning electronic microscope (SEM)). Thin section production and UV fluorescence thin sections were

done at the Shengli Oil Field Analysis and Test Center (Dongying, Shandong Province, China). The thin sections were inspected with both single and cross polarizing microscopes (Karl Zeiss Axio ScopeA1 and Nikon Eclipse E400). Visual estimation was used for the calculation of mineral percentages. The 45 SEM samples were prepared by means of spray-gold on small rock pieces with size ca. 8×8×5 mm, and then analyzed with a Nova Nano SEM 450, within 20 Kv and 15 mtorr. Furthermore, 106 cylindrical samples with diameters of ~2.5 cm and length of ~5 cm were used for measurements of porosity and permeability in order to calibrate the results from the well log petrophysical evaluations (Table 1). The porosity and permeability measurements were conducted on a Porosimeter (YRD-FKS-2) and Relative Permeability Meter (YRD-XDS-3), respectively. The porosity and permeability of the sample is calculated according to the change of the pressure of the gas storage vessel with time and the related parameters. Oil saturation data presented in Table 1 were obtained by nuclear magnetic resonance (NMR) technology, for details of the method seeing in Zhou et al. (2014). Fracture widths were obtained by direct measures on cores, thin sections and FMI logging. The fracture density data were then calculated by means of total fracture numbers per meter.

4. Results

4.1 Lithology and lithofacies

Five different lithofacies types could be found in the eight drill cores taken within the

study area: coherent volcanic, massive tuff, volcanic breccia, tuffaceous sandstone and tuffaceous mudstone lithofacies. All percentages of minerals mentioned in this chapter are to be considered as volume percent. The geochemical compositions of the volcanic rocks are taken from Wang (2018).

Coherent volcanic lithofacies

This lithofacies usually reaches thicknesses of up to 120 m within the wells and drill cores. The rocks appear dense and do not show signs of a brecciated carapace. Vesicles or other characteristic features could not be observed within the samples. Based on geochemical composition, we can subdivide this lithofacies type into three sub-varieties: andesitic, basaltic andesitic and basaltic facies. The andesitic sub-variety (57-63% SiO₂) of this lithofacies (ca. 30%) makes up the major part of the rocks in the drill cores. It exhibits a well-developed porphyritic texture with phenocrysts (varying from 20-35%) of hornblende (5-15%) and plagioclase (15-25%), set in a micro- to cryptocrystalline groundmass (65-80%). Sizes of phenocrysts vary in the range of 0.5-2 mm. The groundmass consists of plagioclase (30-65%) and hornblende (15-35%). The plagioclase microcrystals are randomly distributed and reach a size between 10-200 µm (Fig. 3A-B). The size of the hornblende microcrystals within the matrix is usually 5-20 µm.

A minor portion (ca. 8%) of the volcanic rocks is characterized by lower SiO₂ contents, classifying them as basalts (45-50% SiO₂) and basaltic andesites (50-52%

SiO₂). Like the other andesitic sub-variety, the basaltic and basaltic andesitic sub-variety of this lithofacies also show porphyritic texture. The phenocrysts (ranging from 5-20%) consist of augite (ca. 5%) and plagioclase (ca. 5-15%), set in a micro- to cryptocrystalline matrix (85-95%). The matrix is formed of microcrystalline plagioclase (25-60%), augite (10-25%) and magnetite (5-15%). The size of the phenocrysts varies from 0.5-3 mm. The plagioclase microcrystals within the matrix do not show any alignment and reach sizes of 10-200 µm (Fig. 3C). The augites reach sizes between 5-50 µm.

Due to the dense and coherent appearance and the porphyritic texture, the rocks of this lithofacies have been interpreted as the result of terrestrial lava flows (c.f. Goto et al., 2008).

Volcanic breccia lithofacies

This lithofacies (Fig. 3D-E) makes up the smallest amount of rocks in the drill cores (~10%), reaching thicknesses between 2-10 m. It appears overall massive and does not show signs of any gradation. Their lower and upper contacts with other lithologies are always sharp. Volcanic clasts of basaltic and andesitic composition (2-64 mm in diameter) make up more than 50% of the rock. The clasts are predominantly angular-subangular and are set in a sandy matrix in which preexisting volcanic rocks (~30%), angular plagioclase (~40%), augite (~15%), hornblende (~10%) and lamellar biotite (~5%) can be identified. The degree of sorting is very low.

Due to the poor degree of sorting, angular-subangular shape of the clasts and the massive appearance of this lithofacies, a deposition from debris flows is interpreted (Smith and Lowe, 1991; Coussot and Meunier, 1996; Pierson et al., 1996; Lenhardt et al., 2011). The angular-subangular clasts imply minor abrasion during transport, suggesting a supply of debris from nearby sources (Gihm et al., 2017).

Massive tuff lithofacies

This lithofacies makes up ca. 30% of the drill core material within the study area and is characterized by bright-colors of greyish-green and maroon (Fig. 3F, G). The layers are usually between 5 and 60 cm thick and appear massive without any sedimentary structures. However, superposition of tuff layers may reach thickness of up to 100 m. The SiO₂ content of this lithofacies ranges from 65-80%. It is predominantly formed of broken crystals (15-30%), vitric (pumice, glass shards; ca. 30-50%) and angular lithic fragments (5-10%) and matrix of volcanic dust (ca. 10-20%) (i.e., 5-10% broken crystal, 5-15% vitric and ~ 5% lithic fragment). This lithofacies appears to be well sorted with sizes of its components ranging between 0.1 mm to 2 mm. The crystal fragments are characterized by quartz (ca. 40-60%), plagioclase (ca. 20-30%) and hornblende (ca. 10-20%).

Due to the existence of cusped glass shards, the broken crystals and the angular lithic fragments, the origin of this lithofacies can be interpreted as pyroclastic. The high degree of sorting, the massive appearance with absence of sedimentary structures and

the low thickness of these deposits point to a deposition from pyroclastic fallout (c.f. Lenhardt et al., 2011).

Tuffaceous sandstone lithofacies

This lithofacies makes up ~25% in the observed core material. It generally reaches thicknesses between 20-150 cm. Beds are usually massive and normally graded, however, minor cross beds can also be observed. The lower contacts with underlying tuffs and tuffaceous sandstone are usually concave and sharp. The grains (0.1-2 mm) are predominantly made up of quartz (~50-60%), plagioclase (~10-20%) and lithic fragments (usually volcanic rocks debris, ~20-30%). They are commonly angular to subangular in shape, with a lot of small-scale cracks in quartz grains (Fig. 3H). The grains are cemented by diagenetic minerals such as calcite, sericite and zeolites.

Based on the mineral content, which is similar to that of the massive tuff lithofacies, the original fragmentation process of this lithofacies was pyroclastic (c.f. Lenhardt et al., 2011). Nevertheless, the occurrence of sedimentary structures and the rounding of the fragments point to a reworking of the initial pyroclastic material. The subangular to subrounded shapes of the grains show that the abrasion during transport was rather inefficient. Furthermore, rather brittle minerals such as hornblende are still present. Therefore, a depositional setting proximal to the source area is suggested.

Tuffaceous mudstone lithofacies

This lithofacies takes the minority (only ~5%) in the observed core material (Fig. 3I).

The tuffaceous mudstone in the study area is characterized by brown and greyish-green colour and massive bedding. Thicknesses usually vary from 10 to 50 cm. This lithofacies is interpreted as lacustrine deposit, formed by settling of fine particles through the water column, probably with a large amount of primary or reworked volcanic material (e.g., Fritz and Vanko, 1992).

Based on their eruptional and/or depositional process, the five lithofacies can be grouped into effusive (coherent volcanic) and explosive (massive tuff) volcanic, and epiclastic facies (volcanic breccia, tuffaceous sandstone, and tuffaceous mudstone) that correspond to three depositional stages within the study area (Fig. 4) in ascending order (Wang, 2018):

Stage I: characterized by explosive volcanic facies (in the northwestern and southwestern parts of the study area), effusive volcanic facies (in the southwestern part), and epiclastic facies (in the northeastern part);

Stage II: characterized by effusive volcanic facies (in the southern part), and explosive volcanic facies (in the northern part);

Stage III: characterized by effusive volcanic facies (in the central part), explosive volcanic facies (in the northwestern part), and epiclastic facies (in the northeastern part).

Generally, the Carboniferous volcanic rocks exhibit a N-S striking direction and are distributed along distance of 50 km 50 km. Effusive and explosive volcanic facies can predominantly be found in the east, whereas a shift to epiclastic rocks can be observed towards the west.

4.2 Volcanic reservoir properties

4.2.1 *Types of pore space*

The pore space in the CF Oilfield is characterized by primary and secondary porosities, i.e. the porosity preserved from deposition and lithification, and the pore spaces that formed later through alteration, dissolution and fracturing (cf., Sruoga et al., 2004; Sruoga and Rubinstein, 2007; Lenhardt and Götz, 2011). Primary porosities within the oilfield rocks consist of intercrystal and intergranular pores, and micropores. The secondary porosities are characterized by unfilled fractures and solution pores. Volcanic rocks usually develop into fractured reservoirs, which deliver high short-term but rapidly decreasing production (Li et al., 2015).

The types of pore spaces in the studied rock samples vary in relationship to different lithofacies types (Fig. 5). Pore spaces of the effusive and explosive volcanic facies are

dominated by micropores (Figs. 6A, B), intercrystal pores, fractures (Figs. 6C-G) and solution pores (Figs. 6H, I). On the other hand, micropores provide the only pore space (and reservoir space) within the epiclastic facies, particularly the tuffaceous sandstone and tuffaceous mudstone.

Intercrystal pores are most prominent in the rocks of the coherent volcanic facies and can be found in between the phenocrysts. The intercrystal pores commonly exhibit diameters of 0.01-0.02 mm. Micropores with diameters of 5-50 μm have been observed in the matrix of andesitic and basaltic lava as well as the tuff samples. SEM and image analyses indicate that the intracrystal and micropores at 855.5 m in Well CF70, with a surface porosity of 10%, can serve as an effective reservoir space. Core and microscopic observations show that the solution pores in the volcanic reservoirs are diverse in form, size and shape. Based on logging data, the solution pores are found with high acoustic velocity logging (AC), compensated neutron porosity logging (CNL), and low density logging (DEN), and present irregular spots or bands on the Fullbore Microscan Imager (FMI) imaging logging curves (Fig. 7). The volcanic rocks within the study area contain a large quantity of basic plagioclase (laboradorite, bytownite and anorthite) and unstable mafic minerals (augite, hornblende and biotite), which constitute the petrophysical basis for the occurrence of dissolution and the formation of secondary pore space (Meng et al., 2014). The occurrence of dissolution may be related to long-term surface exposure and the impact of meteoric water infiltration into the volcanic reservoirs below the unconformity, which may have caused the partial dissolution of plagioclase and the mafic minerals

(augite, hornblende and biotite) (c.f. La Felice et al., 2014). An alternative explanation may be that the hydrocarbon generation by mature kerogens in the eastern Changji sag may have released organic acid, which could then have migrated into the volcanic rocks along the Hongche Fault dissolve the unstable minerals, thus leading to the formation of solution pores. Normally, asphaltic residues are preserved in such solution pores, recording the trace of hydrocarbon migration (Hong, et al., 2007). However, light crude filling in the solution pores of the analyzed samples suggest that the crude oil may have rather been generated from younger source rocks instead of asphaltic residues from pre-existing petroleum pores.

4.2.2 Fracture characterization

Both filled and unfilled fractures are well developed in the studied rocks. The unfilled fractures include structural fractures and solution-enlarged tectonically driven fractures (Fig. 6). Statistics on stained thin sections show that the fractures in the Carboniferous volcanic rocks are dominated by structural fractures (73.8%), followed by solution-enlarged tectonically driven fractures (22.2%)- Structural fractures developed mainly in the andesitic lavas (37.5%) (basaltic lava exhibits 11.2% of the fractures) and tuffs (21.1%), followed by the volcanic breccia (13.8%), tuffaceous sandstone (9.9%) and tuffaceous mudstone (6.5%).

Fracture frequencies (number per meter) in andesite, volcanic breccia and tuff are 18.5/m, 15/m and 14/m, respectively (usually less than 5/m in tuffaceous sandstone

and 3/m in tuffaceous mudstone). The length of the fractures generally varies from 1-90 cm. In the andesitic lavas the lengths of the fractures are 8-30 cm, in tuff 1-90 cm and volcanic breccias 3.5-35 cm (usually less than 5 cm in tuffaceous sandstone and tuffaceous mudstone). The width of the fractures varies from 0.01-15 mm with 0.01-8 mm in the andesitic lavas, 0.01-15 mm in tuff and 0.01-5 mm in volcanic breccias (usually in 0.01-0.5 mm in tuffaceous sandstone and less than 0.1 mm in tuffaceous mudstone). Statistically, over 80% of the structural fractures vary from 0.1-0.2 mm, which shows that the structural fractures are dominated by small fractures.

The structural fractures mostly extend in the following directions: E-W, NWW, NW-NNW, NNE and NE. They were mainly formed within three different stages: (1) During the early stage of middle-late Hercynian activity, the Chepaizi area was thrust to the east under NW and NE direction extrusion stress, causing the formation of the N-S trending Hongche fault. The formation of structural fractures during this geological time span is mainly attributed to the eastern part of the study area with a series of X-conjugate shear fractures in EW and NWW directions (Niu et al., 2017). Characteristics of the fracture morphology of this period are irregular, short extensions on a small scale and partial filling with chlorite, quartz or calcite. (2) During Indosinian activity, the Chepaizi area was compressed again by NW directed pressure. A series of NE trending thrust faults came into being during this time. Furthermore, high angle X-conjugate shear cracks in directions of NW and NNW were formed in the study area (Niu et al., 2017) and a series of NNE shear fractures

associated with NE faults was generated within sustainable compressional tectonic stress. The fractures that formed during this period are primarily flat and characterized by long and wide extensions and partial filling with calcite and pyrite. The Indosinian was the main period of structural fracture formation in the study area. Finally, (3) during the late stage of the Yanshan movement period the Chepaizi area was controlled by the NE compressional stress, forming a series of NW trending thrusts, and resulting in the NE shear fractures and small fractures with associated NW faults. The fractures formed at this stage are characterized by small scale width and length, are less in number than the first two stages and partially filled (Wang, 2018).

The core from Well CF70 reveals X-shaped shear structural fractures, showing brownish crude oil in uneven distribution as spots along the fractures. These structural fractures were modified by later hydrothermal flow, which caused secondary change and dissolution of unstable minerals (augite, hornblende and biotite not only as phenocrysts but also in the groundmass). As a result, solution-enlarged tectonically driven fractures came into being irregularly with no special direction.

The channel pore spaces are exhibiting irregular form and are mainly developed near the unconformity on the top of the volcanic succession. They are usually interconnected with solution pores and structural fractures (Chen et al., 2017; Jiang et al., 2017). The channel pore spaces are completely or partially filled with calcite, hematite and limonite, and their unfilled parts may provide pathways for acid fluid flow into the reservoir.

4.2.3 Porosity and permeability

According to measurements and statistics (Table 1; Fig. 8), the porosity of the studied rocks ranges from 1.69-18.13%, with an average of 8.03%. The permeability generally ranges from 0.01×10^{-3} to $4.17 \times 10^{-3} \mu\text{m}^2$, with an average of $0.11 \times 10^{-3} \mu\text{m}^2$. The mean porosities and permeabilities are 8.70% and $0.13 \times 10^{-3} \mu\text{m}^2$ for the explosive volcanic facies, 9.51% and $0.13 \times 10^{-3} \mu\text{m}^2$ for the effusive volcanic facies, and 3.73% and $0.06 \times 10^{-3} \mu\text{m}^2$ for the epiclastic facies, respectively. The results show that porosity and permeability of the tuff samples are most favorable and that this lithofacies may form the best reservoir rock in the study area (before the basaltic and andesitic lavas). The volcanic breccia lithofacies can be considered as a poor reservoir rock. The lowest reservoir qualities are exhibited by the tuffaceous sandstone.

4.3 Oil testing data

Among the CF Oilfield volcanic rocks, the oil saturation ranges between 20-60% (Table 1). Generally, oil saturation in tuff is the highest (40-60%), followed by basaltic (30-50%) and andesitic lavas (25-48%). Volcanic breccias (20-45%) and tuffaceous sandstones (20-40%) show the lowest amounts of oil saturation. Fluorescent thin sections also clarify the good oil-bearing potential in reservoir with favorable matrix and micro-fractures.

5. Discussion

5.1 Controls of reservoir properties of the volcanic rocks

5.1.1 *Lithologic controls on porosities of volcanic rocks*

In the course of this study it was found, that the explosive volcanic facies exhibits the largest porosities and permeabilities, closely followed by the effusive volcanic facies and the epiclastic facies. The same patterns can be seen in the fracture development of these facies (Figs. 8 and 9). In combination with oil saturation data (Table 1), it can be concluded that the most potential hydrocarbon reservoir within the Chunfeng Oilfield is represented by the explosive facies, indicating that the tuffs are best suited for hydrocarbon accumulation. The results of this contribution therefore show that volcanic reservoir space types and their development levels are closely related to the lithologies and lithofacies of their host rocks (c.f. Li, 2013).

5.1.2 *Tectonic controls on the volcanic reservoir properties*

A sufficient hydrocarbon source is essential for hydrocarbon accumulation in volcanic rocks (Zou et al., 2008). This is also true for the CF Oilfield. In the Changji sag, the source rocks are well known for their gas generation potential (Hong et al., 2007). The results of this study show that the distance from the source rocks to the trap is long (ca. 60-140 km; Fig. 1), suggesting long migration and hydrocarbon accumulation outside the source rock. Therefore, the factors that influence the hydrocarbon accumulation include the existence of good migration pathways connecting trap to the source rock.

According to field investigation and seismic profile analysis, the faults in the study area may have been these channels that provided pathways for the upward migration of hydrocarbons. The faults can be divided into three major classes (Fig. 10): Class I faults are represented by the Hongche fault, a deep and large fault, which separates the Chepazi uplift from the Changji sag. Class II faults refer to small reverse faults in the Carboniferous rocks. They commonly extend in NW-SE, and roughly N-S and W-E directions (on average for 3 km). Class III faults are shallow faults in the formations overlying the Carboniferous and inherit the framework of the Carboniferous buried hills with large dip angles and strong opening potential (Ding et al., 2016). The tectonic control on reservoir properties of the volcanic reservoirs is not only the faults alone, but also the tectonic fractures near to the fault system where fractures are prone to forming. Fault associated tectonic fractures are well developed in the intensive tectonic stress fields. The structural fractures form the major reservoir permeability and migration channels of petroleum in the Carboniferous volcanic reservoirs in the study area.

Analysis of core and well logging data indicates that the oil-bearing potential of the volcanic reservoirs in the study area mainly depends on development of fractures. No oil and gas shows could be found in porous reservoirs without any fractures (Figs. 3 and 6), which implies fractures are vital to petroleum migration and accumulation.

5.1.3 Diagenetic controls on the volcanic reservoirs properties

Presence of solution-enlarged pores is usually a favorable condition that improves the petrophysical properties of sandstone reservoirs (Yang et al., 2014; Fan et al., 2017). This is also true for the study area where solution-enlarged pores form an important additional pore space within the Carboniferous rocks (Fig. 11A-C). The pores not only increase the total reserve space of petroleum, but also increase permeability of volcanic rocks when they are connected with each other or linked by tectonic fractures and solution-enlarged tectonically driven fractures (Fig. 11D-F).

5.1.4 Weathering crust controls on the volcanic reservoirs

Core observation reveals obvious and intense weathering leaching at different depths beneath the Carboniferous top weathering crust, where various secondary pores and fractures exist. The more distal to weathering crust, the smaller is the porosity (Fig. 12) and permeability. This indicates that the petrophysical properties of the Carboniferous volcanic reservoirs are controlled by weathering leaching. The volcanic reservoir in the weathering leaching belt near the unconformity shows good reservoir properties and a high oil-bearing potential (Fig. 13), and is the primary hydrocarbon accumulation in the study area. Moreover, the oil pay zones decrease further away from the Carboniferous unconformity (Fig. 13), which basically coincides with the vertical thickness distribution of the weathering crust. This implies that the unconformity controls the vertical distribution of the reservoir and it may have been a migration conduit for hydrocarbons.

5.2 Hydrocarbon accumulation models

As discussed above, lithology, tectonics, diagenesis and the weathering crust are all controlling factors for the oil distribution in the CF Oilfield petroleum reservoirs. What is more important, the reservoir quality often has influence on hydrocarbon accumulation models. Among all controlling factors of volcanic rock reservoirs, the oil-bearing potential is mainly controlled by fractures, which form in tectonic stress fields. Specifically, the fractured-porous reservoirs are believed to be of a high oil-bearing potential. This has been proven by drilling and oil production of the CF Oilfield.

As it was shown by UV fluorescent thin sections, there is good oil-bearing potential in reservoirs with favorable fractures. Despite favorable geophysical properties with relatively high porosity of 8.90~9.85 %, the reservoir interval without fractures contains little oil. As an example, Well CF71 with well developed fractures produces 17 m³ oil per day. On the other hand, Well CF61 without fractures only produces a large amount of water but no oil. This indicates that the oil-bearing potential of the volcanic reservoirs in the study area is mainly controlled by fractures. Fractured-porous reservoirs are the most favorable oil-bearing zones. Fractures act as reservoir space and also connect the pores to increase the conductivity (Wang and Yang, 2012). Furthermore, they determine the oil accumulation in the reservoirs and separate the reservoirs into blocks. Additionally, some wells (e.g. CF77) exhibit high but quickly decreasing production performance at an early stage, and low but

long-lasting performance at a later stage (Fig. 14). Both fractures and matrix pores (micropores and intercrystal pores) in the volcanic reservoir contain oil. In the early stage, oil was produced from the fractures at a high rate but reduced quickly. In the late stage, oil was produced from the matrix pores at a low rate, but lasted for long time.

Traps at structural highs contain richer hydrocarbons than those in structural lows (Song et al., 2007; Yuan et al., 2012). In general, the structure in the CF Oilfield is high in the northwest and low in the southeast and on the upthrow side of the Hongche fault. Such structure controls the primary hydrocarbon migration orientation - from low positions to high positions.

The oil-bearing potential and enrichment differs greatly in different stages (Fig.4). Specifically, in stage III, oil layers at higher structural position are thicker and contain more oil and gas. In stage II, oil layers at relatively low positions are thin. In stage I, oil layers are rare, but water layers are predominant.

We present several conceptual geological models of petroleum accumulation in the Carboniferous volcanic reservoir of the study area. In all models, the faults could be considered as the primary pathways for vertical migration of hydrocarbons; the unconformity and skeleton sandstone of the Baodaowan (Lower Jurassic) and Shawan (the Lower Neogene) formations could have enabled the lateral long-distance migration of hydrocarbons, leading to hydrocarbon migration and accumulation in the volcanic rocks (Fig. 15A). These three elements, i.e. fault, unconformity and

sandstone comprise a step-like migration system. In the reservoir above the source rocks, hydrocarbons migrated vertically along Class I faults to the overlying sandstone or unconformity (Fig. 15B, C). In this case, the faults are oil-migrating faults. They provided vertical pathways for oil and gas migration when the hydrocarbon expulsion was in peak at the end of the Triassic. The regional study shows that sandstone bodies with high porosity and permeability, formed in the Jurassic at the downthrown side of oil-migrating faults (Fig. 15B, C), served as a transit for hydrocarbons generated in the source rocks when they migrated to and accumulated in the trap (Chen et al., 2017). Given a favorable contact between sandstone bodies and the unconformity, hydrocarbons would migrate along the unconformity and Class II faults to the structural high and finally accumulate in the Carboniferous rocks (Fig. 15D). Subsequent tectonic movements and hydrocarbons generated at a late stage (from the Jurassic to the present) may have mixed with the original charge of the early accumulations. Oil generated in the Jurassic migrated along Class III faults vertically to the unconformity and the skeleton sandstone. If the sandstone directly connected to the Carboniferous volcanic reservoir, hydrocarbons might also accumulate in the Carboniferous rocks (Fig. 15D). This composite migration system enabled hydrocarbons to migrate laterally to the skeleton sandstone. Thus, the oil-migrating fault, the regional unconformity, and the Jurassic sandstone pathway likely form a composite migration system in the CF Oilfield, which controls the hydrocarbon accumulation and reservoir distribution.

5.3 Recommendations for future exploration

As a result of random seismic reflection of volcanic rocks in the CF oilfield, it is hard to predict petroleum pools only by means of a seismic reflection profile. Thus, geological research based on lithologic and tectonic characteristics of the volcanic rock reservoir is crucial to petroleum exploration in this area. This study shows that tuff and andesite exhibit the best petrophysical properties among all analyzed lithofacies types. Tuff and andesite can easily be recognized on well logs. Furthermore, due to their relatively large spatial extent, less effort may be needed in order to predict the distribution of the two lithofacies. As a result, distribution regulations of these volcanic rocks and reservoirs prediction are reasonably based on well correlations, accompanied with drill cores and seismic data. Thus, in the future, a special focus on these two volcanic lithofacies is recommended.

Besides the lithofacies, special attention should be given to existing fractures, which not only provide pore space, but also act as the main crude oil migration paths. Thus, fractures are important not only for the petroleum accumulation, but also for oil production. Predicting the orientation and distribution of fractures is thus crucial to petroleum exploration.

Fluid charging through migration paths (fault, fractures, skeleton sandstone and high permeability reservoirs) and petroleum accumulation patterns are crucial to reservoir prediction and exploration. For more detailed geochemical studies on the charge origin, charge filling history and possible charge mixing in the reservoirs, the reader is referred to Wang and Yang (2012), Yuan et al. (2012), Wu et al. (2014), Chen et al.

(2016a, 2017) and Wei et al. (2017). As we discussed in section 5.2, there are two preferable petroleum accumulation patterns in the Carboniferous volcanic rocks. The first model favors formation of a petroleum accumulation on conditions (Fig. 15 A) that: 1) the position of the skeleton sandstones is lower than that volcanic rocks; 2) the skeleton sandstones are in contact with the weathering leaching zone; 3) the volcanic rocks are capped by mudstones. The second model is similar to the first one with the exception that here the skeleton sandstone is almost in contact with the volcanic rock reservoirs (Fig. 15D). In the future, petroleum exploration in the Junggar Basin should pay special attention to these two types of geological traps.

6. Conclusions

1) Volcanic reservoirs in the study area are mainly composed of tuff and andesite, with the dominance of explosive and effusive facies. The reservoir space consists of solution pores, unfilled fractures, intercrystal pores, intergranular pores and micropores. The reservoir is highly heterogeneous and characterized by high porosity and low permeability. The oil-bearing potential is controlled by fractures. Effective reservoirs are fractured and fractured with high matrix porosity. No oil/gas shows were found in porous reservoirs based on core and cuttings analyses.

2) Class II and III faults, regional unconformity, and adjoining Jurassic sandstone bodies form the most likely petroleum migration system and are essential for the hydrocarbon accumulation in CF oil field. The tuff of the eruptive facies has the best

petrophysical properties and the highest probability of hydrocarbon accumulation. The configuration of solution pores and fractures in favorable lithology/facies belts determines the high productivity of reservoir, and the intercrystal pores and matrix micropores are very important for the stable production of reservoir.

3) In the study area, the unconformity controls the vertical distribution of the reservoir, demonstrating that the oil pay zones decrease farther from the Carboniferous unconformity. Hydrocarbons may probably accumulate in areas close to structural highs or big faults. In stage III, oil layers at higher structural position are thicker and contain more oil and gas. In stage II, oil layers at relatively low positions are thin. In stage I, oil layers are rare, but water layers are predominant (Fig.4).

4) The tectonic setting controls the orientation of hydrocarbon accumulation. The oil-bearing potential is different in traps at different structural positions. Thus, the structural position and faults control the formation of oil and gas traps, and play a key role in the hydrocarbon accumulation or re-accumulation.

Acknowledgments

This study was supported by the National Natural Science Foundation of China (grant No. 41672120 and No. 41402120), and Shandong University of Science and Technology Research Fund (grant No. 2015TDJH101).

References

Carroll, A.R., Graham, S.A., Smith, M.E., 2010. Walled sedimentary basins of China, in: Graham, S.A., Carroll, A.R., Ping, L. (Eds.), Tectonic and stratigraphic evolution of nonmarine basins of China. *Basin. Res.* 22, 17-32.

Chen, Z., Zha, M., Liu, K., Zhang, Y., Yang, D., Tang, Y., Wu, K., Chen, Y., 2016a. Origin and accumulation mechanisms of petroleum in the Carboniferous volcanic rocks of the Kebai Fault zone, Western Junggar Basin, China. *J. Asian Earth Sci.* 127, 170-196.

Chen, Z., Liu, W., Zhang, Y., Yan, D., Yang, D., Zha, M., Li, L., 2016b. Characterization of the paleocrusts of weathered Carboniferous volcanics from the Junggar Basin, western China: Significance as gas reservoirs. *Mar. Pet. Geol.* 77, 216-234.

Chen, Z. H., Wang, X. Y., Wang, X. L., Zhang, Y. Q., Yang, D. S., Tang, Y., 2017. Characteristics and petroleum origin of the Carboniferous volcanic rock reservoirs in the Shixi Bulge of Junggar Basin, western China. *Mar. Pet. Geol.* 80, 517-537.

Coussot, P., Meunier, M., 1996. Recognition, classification and mechanical description of debris flows. *Earth-Sci. Rev.* 40, 209-227.

Ding, A.J., Zhang, C., Lai, G.H., Guo, C.J., Zhou, Y. J., 2016. Structural characteristics and sedimentary filling characteristics of the Chunguang block in Junggar Basin. *Petrol. Geol. Eng.* 30, 14-17. (in Chinese)

Dong, D.W., Li, L., Wang, X.L., Zhao, L., 2015. Structural Evolution and Dislocation Mechanism of Western Margin Chepaizi Uplift of Junggar Basin. *J. Jilin Uni.: Earth Sci. Ed.* 45, 1132-1141. (in Chinese)

Fan A., Yang R., Li J., Zhao Z., Van Loon, A.J., 2017. Siliceous cementation of chlorite-coated grains in the Permian sandstone gas reservoirs, Ordos Basin. *Acta Geol. Sin.* 91, 11473-1148.

Feng, Z., 2008. Volcanic rocks as prolific gas reservoir: a case study from the Qingshen gas field in the Songliao Basin, NE China. *Mar. Pet. Geol.* 25, 416-432.

Fritz, W.J, Vanko, D.A., 1992. Geochemistry and origin of a black mudstone in a volcanoclastic environment, Ordovician Lower Rhyolitic Tuff Formation, North Wales, UK. *Sedimentology* 39, 663-674.

Gihm, Y.S., Kim, M.-C., Son, M., Hwang, I.G., 2017. The influence of tectonic

subsidence on volcanoclastic sedimentation: The Cretaceous upper Daeri Member, Wido Island, Korea. *Island Arc* 26, e12183. DOI 10.1111/iar.12183.

Goto, Y., Nakada, S., Kurokawa, M., Shimano, T., Sugimoto, T., Sakuma, S., Hoshizumi, H., Yoshimoto, M., Uto, K., 2008. Character and origin of lithofacies in the conduit of Unzen volcano, Japan. *J. Volcanol. Geotherm. Res.* 175, 45-59.

Hao, Y., Zhao, Y., Zhou, M., Li, H., 2004. The reservoir evaluation method for calculating the ratio of porosity to permeability with log data. *Well Log. Tech.* 28, 135-137. (in Chinese)

Hong, T.Y., Wang, L.C., Meng, X.L., Wu, J., 2007. The main control factors of oil and gas Accumulation in Chepaizi area on the western Junggar basin. *Xinjiang Geol.* 25, 389-393. (in Chinese)

Hou, L.H., Luo, X., Wang, J.H., Yang, F., Zhao, X., Mao, Z.G., 2013. Weathered volcanic crust and its petroleum geologic significance: A case study of the Carboniferous volcanic crust in northern Xinjiang. *Petroleum Exploration and Developmen.* 31, 257-265.

Jiang, F., Cheng, R.H., Ruan, B.T., Lin, B., Xu, Z.J., Li, Z.C., 2017. Formation mechanism of volcanic reservoirs within a volcanostratigraphic framework: The case of the Wangfu fault depression in the Songliao Basin, China. *Mar. Pet. Geol.*, 84, 160-178.

La Felice, S., Montanari, D., Battaglia, S., Bertini, G., Gianelli, G., 2014. Fracture permeability and water-rock interaction in a shallow volcanic groundwater reservoir and the concern of its interaction with the deep geothermal reservoir of Mt. Amiata, Italy. *J. Volcanol. Geotherm. Res.* 284, 95-105.

Landes, K.K., Amoruso, J.J., Charlesworth, Jr., L.J., Heany, F., Lesperance, P.J., 1960. Petroleum Resources in Basement Rocks. *Am. Assoc. Pet. Geol. Bull.* 44, 1682-1691.

Lenhardt, N., Götz, A.E., 2011. Volcanic settings and their reservoir potential: An outcrop analog study on the Miocene Tepoztlán Formation, Central Mexico. *J. Volcanol. Geotherm. Res.* 204, 66-75.

Lenhardt, N., Götz, A.E., 2015. Geothermal reservoir potential of volcanoclastic settings: The Valley of Mexico, Central Mexico. *Renew. Energ.* 77, 423-429.

Lenhardt, N., Hornung, J., Hinderer, M., Böhnel, H., Torres-Alvarado, I.S., Trauth, N., 2011. Build-up and depositional dynamics of an arc front volcanoclastic complex: The Miocene Tepoztlán Formation (Transmexican Volcanic Belt, Central Mexico). *Sedimentology* 58, 785-823.

Levin, L.E., 1995. Volcanogenic and volcanoclastic reservoir rocks in Mesozoic-Cenozoic island arcs: Examples from the Caucasus and the NW Pacific. *J. Pet. Geol.* 18, 267-288.

Li, G.L., 2013. Analysis of Carboniferous igneous hydrocarbon accumulation characteristics and controlling factors on Hashan region. *China Univ. of Petrol.* (in Chinese)

Li, J., Xue, P., Zhang, A., Liu, X., 2008. Characteristics and controlling factors of Carboniferous volcanic reservoir in the middle section of the northwestern margin of Junggar Basin. *Acta Pet. Sin.* 29, 329-335. (in Chinese)

Li, J., Zhang, J.H., Han, S., Zhu, W.B., Yang, Y., Du, Y.S., 2015. A review: exploration status, basic characteristics and prediction approaches of igneous rock reservoir. *Geophys. Prospect.* 50, 382-392. (in Chinese)

Luo, X., Gong, S., Sun, F.J., Wang, Z.H., Qi, J.S., 2017. Effect of volcanic activity on hydrocarbon generation: Examples in Songliao, Qinshui, and Bohai Bay Basins in China. *J. Nat. Gas Sci. Eng.* 38, 218-234.

Magara, K., 2003. Volcanic reservoir rocks of northwestern Honshu island, Japan. *Geol. Soc. Spec. Publ.* 214, 69-81.

Meng, Y.L., Hu, Y., Li, X.N., Hu, A.W., Wu, C.L., Zhao, Z.T., Zhang, L., Xu, C., 2014. Controlling factors on physical properties of tight volcanic rocks and reservoir quality prediction: a case study of the Tiaohu Formation in Marlang-Tiaohu Sag. *Oil & Gas Geol.* 35, 244-252. (in Chinese)

Nayoan, G.A.S., 1981. Offshore hydrocarbon potential of Indonesia. *Energy* 6, 1225-1246.

Niu, H., Yang, S., Wang, Y., He, N., Ma, B., 2017. Analysis on the formation periods of fractures of volcanic reservoirs in Chepaizi area, Junggar Basin. *Natur. Gas Geosci.* 28, 74-81. (in Chinese)

Pierson, T.C., Daag, A.S., Reyes, P.J.D., Regalado, M.T.M., Solidum, R.U., Tubianosa, B.S., 1996. Flow and deposition of post-eruption hot lahars on the east side of Mount Pinatubo, July-October 1991, in: Newhall, C.G., Punongbayan, R.S. (Eds.), *Fire and Mud, Eruptions and Lahars of Mount Pinatubo, Philippines*. Philippines Institute of Volcanology and Seismology, Univ. Washington Press, Seattle, 921-950.

Qiu, Z., Zou, C., Dong, D., Lu, B., Shi, Z., Tao, H., Zhou, J., Lei, D., Zhang C., 2016. Petroleum system assessment of conventional-unconventional oil in the Jimusar sag, Junggar basin, Northwest China. *J. Unconvent. Oil Gas Res.* 16, 53-61.

Sakata, S., 1997. Geochemistry of natural gases from the green tuff region, Japan - Basic study on the origin of light hydrocarbons in volcanic reservoir rocks. *Sekiyu Gakkaishi. J. the Japan Petrol. Instit.* 40, 260-262.

Schutter, S.R., 2003a. Hydrocarbon occurrence and exploration in and around igneous rocks, in: Petford, N., McCaffrey, K.J.W. (Eds.), *Hydrocarbons in crystalline rocks*. Geol. Soc. London Spec. Publ. 214, 7-33.

Schutter, S.R., 2003b. Occurrences of Hydrocarbons in and around Igneous Rocks, in: Petford, N., McCaffrey, K.J.W. (Eds.), *Hydrocarbons in crystalline rocks*. Geol. Soc. London Spec. Publ. 214, 35-68.

Sembodo, I., 1973. Notes on formation evaluation in the Jatibarang volcanic reservoir. Proc. Annual Conv.—Indon. Petrol. Assoc., 131-147.

Shi, J., Sun, G., Zhang, S., Guo, H., Zhang, S., Du, S., 2017. Reservoir characteristics and control factors of Carboniferous volcanic gas reservoirs in the Dixi area of Junggar Basin, China. J. Nat. Gas Geosci. 2, 43-55.

Smith, G.A., Lowe, D.R., 1991. Lahars: volcano-hydrologic events and deposition in the debris flow – hyperconcentrated flow continuum, in: Fisher, R.V., Smith, G.A. (Eds.), Sedimentation in Volcanic Settings. SEPM Spec. Publ. 45, 59-70.

Song, C.C., He, L.J., Ma, L.G., Ren, H.N., Zhu, G., 2007. Characteristic of Hydrocarbon Accumulation of Chepaizi uplift in Junggar Basin. Xinjiang Petrol. Geol. 28, 136-138. (in Chinese)

Sruoga, P., Rubinstein, N., 2007. Processes controlling porosity and permeability in volcanic reservoirs from the Austral and Neuquén basins, Argentina. AAPG Bull. 91, 115-129.

Sruoga, P., Rubinstein, N., Hinterwimmer, G., 2004. Porosity and permeability in

volcanic rocks: a case study on the Serie Tobífera, South Patagonia, Argentina. *J. Volcanol. Geotherm. Res.* 132, 31-43.

Tang, Z.-H., Parnell, J., Longstaffe, F.J., 1997. Diagenesis and reservoir potential of Permian-Triassic fluvial/lacustrine sandstones in the southern Junggar Basin, northwestern China. *AAPG Bull.* 81, 1843-1865

Tang, H., Yang, D., Shao, M., Wang, P., Sun, W., Huang, Y., 2016. Constraint of volcano-stratigraphic emplacement environment on the reservoir distribution: A case analysis of rhyolitic volcanic strata in the 2nd member of Jurassic Huoshiling Formation in Wangfu fault depression, Songliao Basin, East China. *Petrol. Explor. Dev.* 43, 626-633.

Tao, G, Hu, W., Zhang, Y., Cao, J., Zhang, Y., Gao, X., 2006. NW-trending transverse faults and hydrocarbon accumulation in the northwestern margin of Junggar Basin. *Acta Pet. Sin.* 27, 23-28.

Wang, Y., 2018. Forming mechanism of fractures in the Carboniferous volcanic rocks and its controls on petroleum accumulation in the Chepeizi area, Junggar Basin. PhD thesis of China University of Petroleum. (in Chinese)

Wang, J.H., Yang, F., 2012. Adjusting and Controlling Effect of Chepaizi-Mosuowan Paleo-uplift on Paleo-reservoir and Hydrocarbon Accumulation. *J. Southwest Petrol. Univ. (Sci. Tech. Ed.)* 34, 49-58. (in Chinese)

Wang, K., Liu, W., Huang, Q.Y., Shi, S.Y., Ma, K., Liang, D.X., 2015. Development Characteristics and Evolution of the Cambrian Sedimentary System in Tazhong and Gucheng Area, Tarim Basin. *Geol. Sci. Tech. Infor.* 34, 116-124. (in Chinese)

Wei, Y., Zhao, X., Lu, S., Zhao Z., Comparison of geochemical characteristics and forming environment of volcanic rocks in Northern Xinjiang and the Songliao Basin, China. *J. Nat. Gas Geosci.* 2, 119-130.

Wu, K.J., Liu, L.F., Zeng, L.Y., Gao, X.Y., Xu, Z.J., Zhou, C.X., 2014. Hydrocarbon migration in the Neogene Shawan Fm. sandstone around Chepaizi uplift, Junggar Basin. *J. Cent. South Univ. (Sci. Tech.)* 45, 4258-4266. (in Chinese)

Yang, R., Fan, A., Van Loon, A.J., Han, Z., Wang, X., 2014. Depositional and Diagenetic Controls on Sandstone Reservoirs with Low Porosity and Low Permeability in the Eastern Sulige Gas Field, China. *Acta Geol. Sin.* 88, 1513-1534.

Yuan, L., Ren, X.C., Mu, Y.Q., Cheng, C.L., Shang, F.K., Guan, C.P., 2012. Oil-gas

conducting System in Chunfeng Oilfield in Junggar Basin. *Xinjiang Petrol. Geol.* 33, 288-289. (in Chinese)

Zhang, S.W., Yang, Y.H., 2016. The method and practice of fine exploration in the mature oilfield of Shengli. *China Offshore Oil and Gas* 28, 37-44. (in Chinese)

Zhang, Z.H., Liu, H.J., Li, W., Fei, J.J., Xiang, K., Qin, L.M., Xi, W.J., Zhu, L., 2014. Origin and Accumulation Process of Heavy Oil in Chepaizi Area of Junggar Basin. *J. Earth Sci. Envir.* 44, 18-32. (in Chinese)

Zhao, W.Z., Zou, C.N., Li, J.Z., Feng, Z.Q., Zhang, G.Y., Hu, S.Y., Kuang, L.C., Zhang, Y., 2009. Comparative study on volcanic hydrocarbon accumulations in western and eastern China and its significance. *Petrol. Explor. Develop.* 36, 1-11.

Zhou, S., Guo, H., Xue, H., Guo, W., 2014. Comprehensive testing for oil saturation parameters in reservoirs based on NMR technology. *Sci. Tech. Eng.* 14, 224-229. (in Chinese)

Zou, C.N., Zhao, W.Z., Jia C.Z., Zhu, R.K., Zhang, G.Y., Zhao, X., Yuan, X.J., 2008. Formation and distribution of volcanic hydrocarbon reservoirs in sedimentary basins in China. *Petrol. Explor. Develop.* 35, 257-271. (in Chinese)

About the author: Wang Yong (1979-), male, born in Feicheng County, Shandong Province, doctoral candidate, is engaged in the theory, methods and technology research for oil and gas resources exploration. He obtained a doctorate degree.

Contact: **E-mail:** 420260511@qq.com **Tel:** 18754601877

Figure captions:

Fig. 1. Basinal location, geological setting, well locations and strata of the study area.

A. Location of the Junggar Basin in the northwestern part of China, and location of insert map B; B. Tectonic division of the western part of the Junggar Basin and its surrounding mountains, and location of the study area (Chunfeng Oilfield, or Chepaizi Uplift); C. well locations, sampling locations and field profile locations, as well as ranges of the oilfield, fault and burial contour lines; D. Strata of the northwestern Junggar Basin.

Fig. 2. Lithology column of the Carboniferous System in the western Junggar Basin (A), and lithology column and logging curves of the target--Xibeikulasi Formation (B).

Fig. 3. Lithological characteristics of the Carboniferous volcanic rocks in the CF oilfield. A. Porphyritic texture of an andesite, shows solution pores in augite phenocrysts (yellow arrows), well P66, in depth of 1061.18 m, plane-polarized light; B. Porphyritic texture of an andesite, solution pores can be seen at yellow arrows, well P662, in depth of 1093.32 m, cross-polarized light; C. Porphyritic texture of a basalt, shows solution pores in augite phenocrysts (yellow arrows), well P666, in depth of 1070.2 m, plane-polarized light; D. Pores and holes in a core of volcanic breccia (yellow arrows), well P66, in depth of 1206.30-1206.42 m; E. Pores and holes in a core (yellow arrows) of volcanic breccia, with oil spot (white arrows), well P66, in depth of 1206.30 m; F. Structural fractures in tuff, well P61, in depth of 1001.90 m; G. Channel pore spaces in tuff, well P 60, in depth of 620.50 m; H. Structural fractures in tuffaceous sandstone, well P60, in depth of 621.30 m, plane-polarized light; I. Solution-enlarged tectonically driven fractures in tuffaceous mudstone, well P60, in depth of 618,60 m, plane-polarized light.

Aug, augite; Lau, laumontite; I, illite; Q, quartz; F, feldspar.

Fig. 4. Profile of the Carboniferous volcanic rock reservoirs in the CF Oilfield (for location of the profile, refer to Fig. 1).. It also shows the weathering crusts (unconformities) among the Carboniferous, Jurassic and Cretaceous, and three stages of volcanic activities. The first stage of volcanic eruption was dominated by basalts and tuffs with a minority of volcanic breccias. The second stage was mainly made up of basalts and tuffs, which later on developed solution pores. The third stage of volcanic eruption was dominated by andesites and tuffs, with a minority of basalts. Petroleum (in red) mainly accumulated in the third and the second stages of volcanic

rocks, which is near to the uppermost weathering crust of the Carboniferous volcanic rocks or near to faults and fractures.

Fig. 5. Volcanic facies, lithology, main reservoir spaces and their logging response in the Carboniferous volcanic rocks, well P61, Xibeikulasi Formation, CF Oilfield.

Fig. 6. Different scales of fractures in the Carboniferous volcanic rocks in the CF oilfield. A. Intercrystalline micro-pores (yellow arrow) and intracrystalline solution micro-pore (white arrow), well P61, in depth of 855.5 m, SEM photo; B. Intercrystalline micro-pores (yellow arrow), well P61, in depth of 855.5 m, SEM photo; C. Structural fractures in tuff, well P665, in depth of 795.28 m, plane-polarized light; D. Structural fractures in tuff, well P624, in depth of 962.45 m, plane-polarized light; E. Solution-enlarged tectonically driven fractures in sedimentary tuff, well P665, in depth of 791.05 m, plane-polarized light; F. Channel pore spaces in sedimentary tuff, well P60, in depth of 620.56 m, plane-polarized light; G. Solution-enlarged tectonically driven fractures in sedimentary tuff, well P666, in depth of 982.01 m, UV fluorescence photo. H. A few pores containing crude oil in sedimentary tuff, well P665, in depth of 852 m, fluorescence photo; I. Solution pore and crude oil in a sedimentary tuff, well P666, in depth of 1067 m, UV fluorescence photo.

Fig. 7. Lithologic column, well logs and measurements of fractures, well P61, [Xibeikulasi formation](#), CF Oilfield. PE is photoelectric absorption cross-section index. Fracture width and length were obtained by direct measurement on cores, thin

sections and FMI logging. Fracture density is calculated by ratio of fracture numbers per meter. Fracture porosity was calculated by fracture width and length. Fracture intensity index is the ratio of fracture porosity to total porosity.

Fig. 8. Histograms of porosity, permeability, fracture width and fracture density for the Carboniferous volcanic rocks in the CF Oilfield. Porosity and permeability are determined from core samples measurement and downloaded from the database of the Shengli Oilfield Company. Fracture width and density are determined from measurement on cores, thin sections and FMI log, and downloaded from the database of the Shengli Oilfield Company.

Fig. 9. Lithologic column, logging curves, FMI logging and calculated porosity and permeability of well P66, CF Oilfield.

Fig. 10. Seismic profile with interpreted fault system and strata (for location of the seismic profile, refer to Fig. 1).

Fig. 11. Solution pores in the Carboniferous volcanic rocks, plane-polarized light, stained thin sections. A. micro-pores formed by devitrification of pyromeride (yellow arrow) and solution pores (white arrows), well QH3, in depth of 2686.95 m; B. Solution pores (yellow arrows) in Pyroxene phenocrysts of Basaltic breccia lava, well P 667, in depth of 993.40 m; C. Solution pores (yellow arrows) in matrix of Basaltic

breccia lava, well P 672, in depth of 1153.54 m; D. Solution pores of calcite cement in fracture of Basaltic breccia lava, well HS2, in depth of 1209.54 m; E. Solution pores (yellow arrows) of calcite cement in amygdaloidal stomatal andesite, well HS1, in depth of 111.72 m; F. Pores of devitrification of volcanic glass (yellow arrow) and solution-enlarged tectonically driven fractures (white arrows), well P66, in depth of 2605.60 m.

Fig. 12. Porosity measured from core samples of the Carboniferous volcanic rocks and their distances away from the uppermost weathering crust.

Fig. 13. Oil saturation of the Carboniferous volcanic rock reservoirs in relationship to the distance away from the topmost weathering crust.

Fig. 14. Daily oil and water production of fractured reservoir in Well P663 in the CF Oilfield.

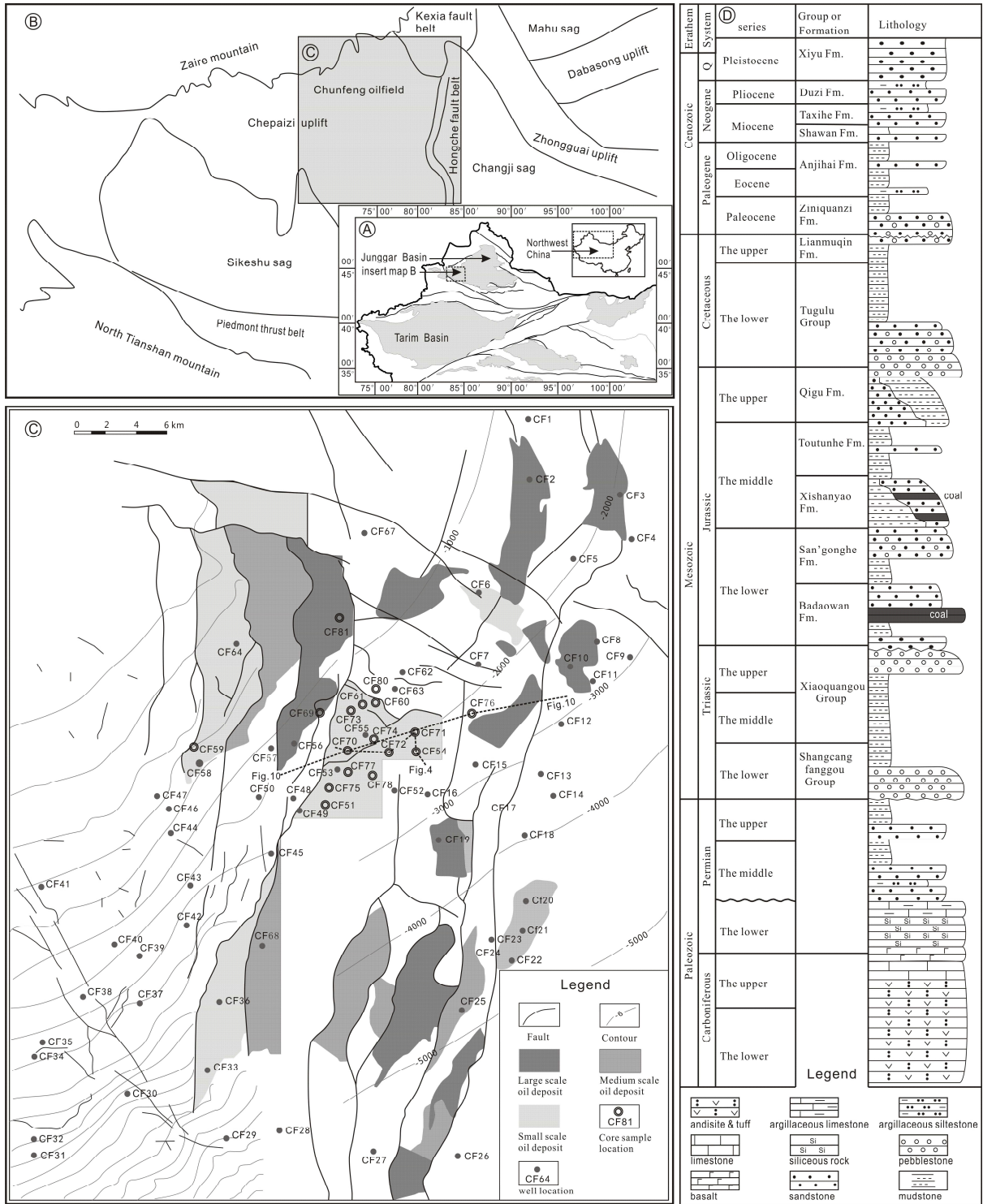
Fig. 15. Idealized models of petroleum accumulation related to the Carboniferous volcanic rocks and its topmost weathering crust. A) Petroleum accumulation pattern of isolated volcanic rocks and sandstone (IVRS). Hydrocarbon migrated through sandstone and unconformity surface, and accumulated in the weathering leaching zone in the Carboniferous volcanic rocks. B) Hydrocarbon accumulated in sandstone reservoirs and trapped by the Carboniferous top hard crust. C) Hydrocarbon migrated

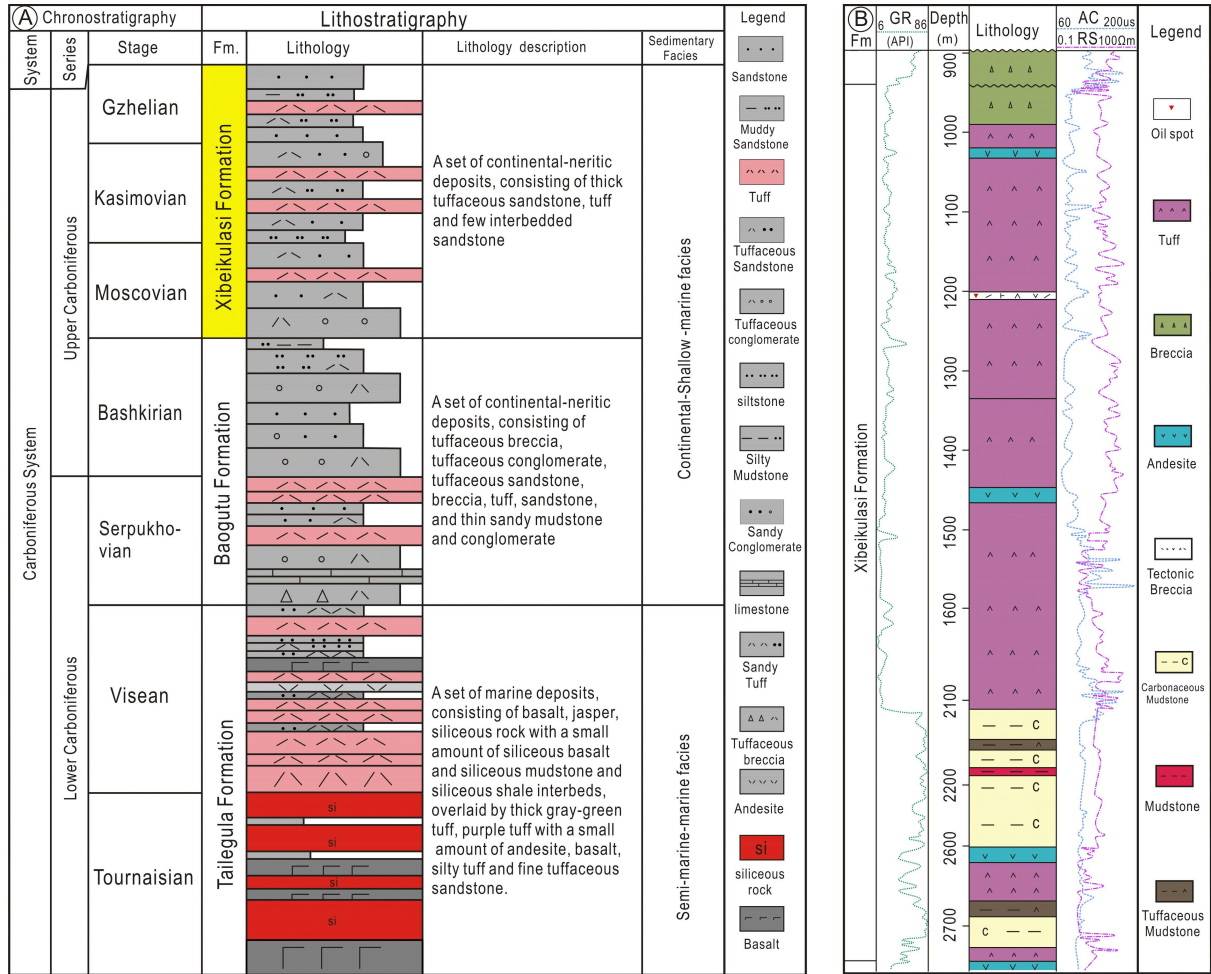
through sandstone and volcanic rocks, and accumulated in the top most of sandstone reservoirs (N_1S_1). D) Petroleum accumulation pattern of connected volcanic rocks and sandstone (CVRS). Hydrocarbon migrated through sandstone and volcanic rocks, and accumulated in the top of the Carboniferous weathering leaching zone.

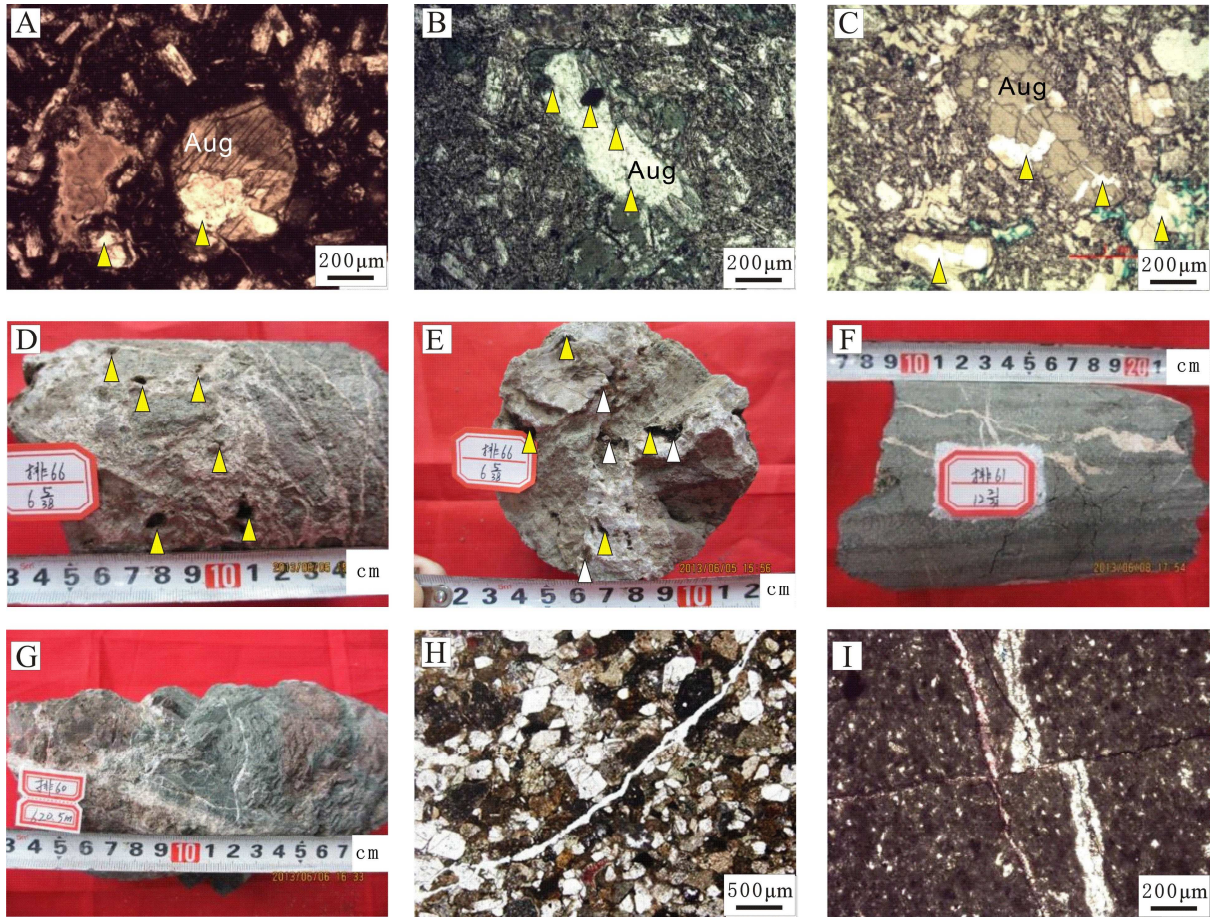
Table captions:

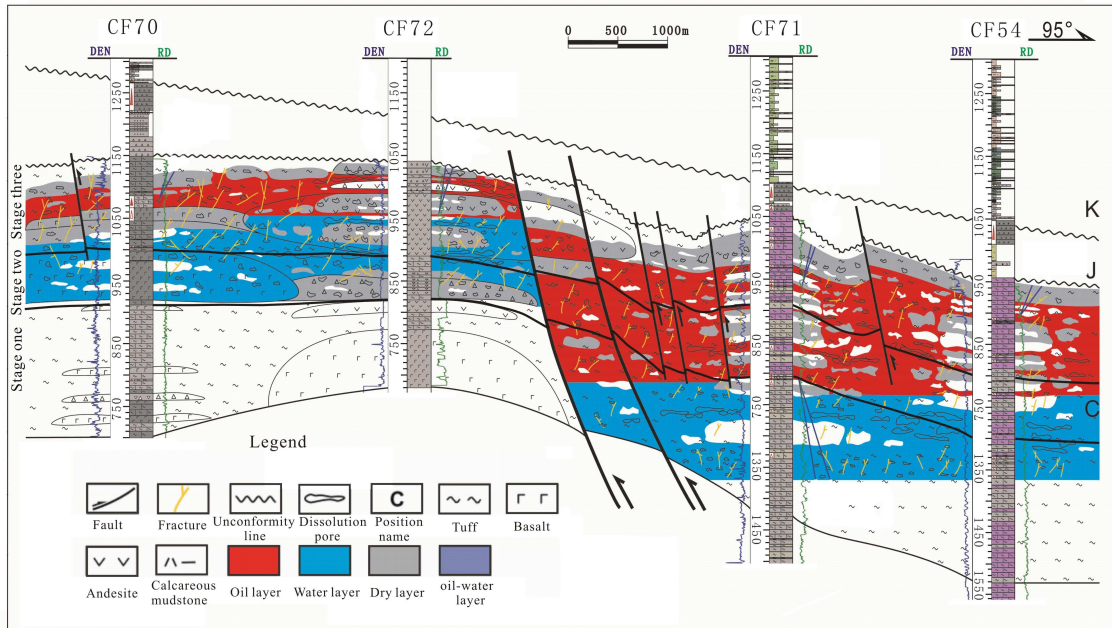
Table 1. Lithology, porosity, permeability, and oil saturation of the Carboniferous volcanic rock reservoirs in the CF Oil field, Junggar Basin.

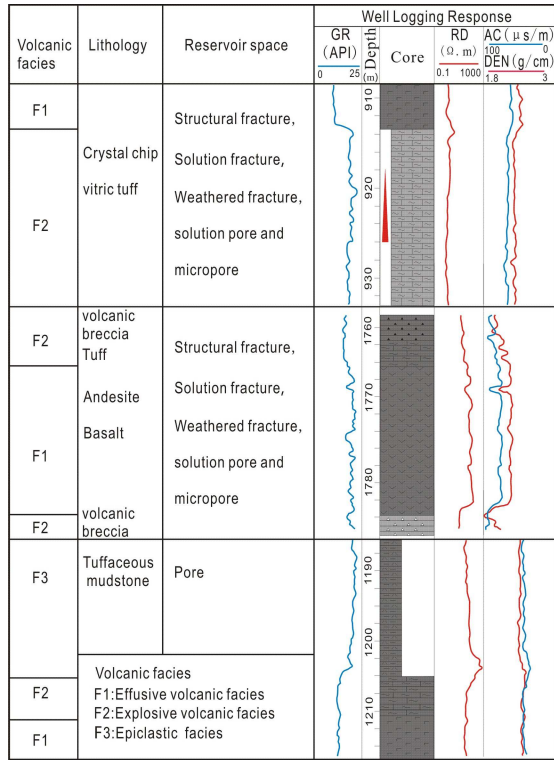
lithofacies	number of measurements	range of porosity (%)	porosity mean (%)	range of permeability ($\times 10^{-3} \mu\text{m}^2$)	permeability mean ($\times 10^{-3} \mu\text{m}^2$)	oil saturation (%)
basalt	15	3.98-13.52	9.67	0.05-1.76	0.14	30~50
andesite	22	3.65-12.89	9.34	0.04-1.63	0.11	25~48
tuff	37	5.91-18.13	11.23	0.06-4.17	0.19	40~60
volcanic breccia	21	2.35-11.07	6.16	0.01-2.35	0.07	20~45
Tuffaceous sandstone	11	1.69-9.14	3.73	0.01-1.13	0.06	20~40

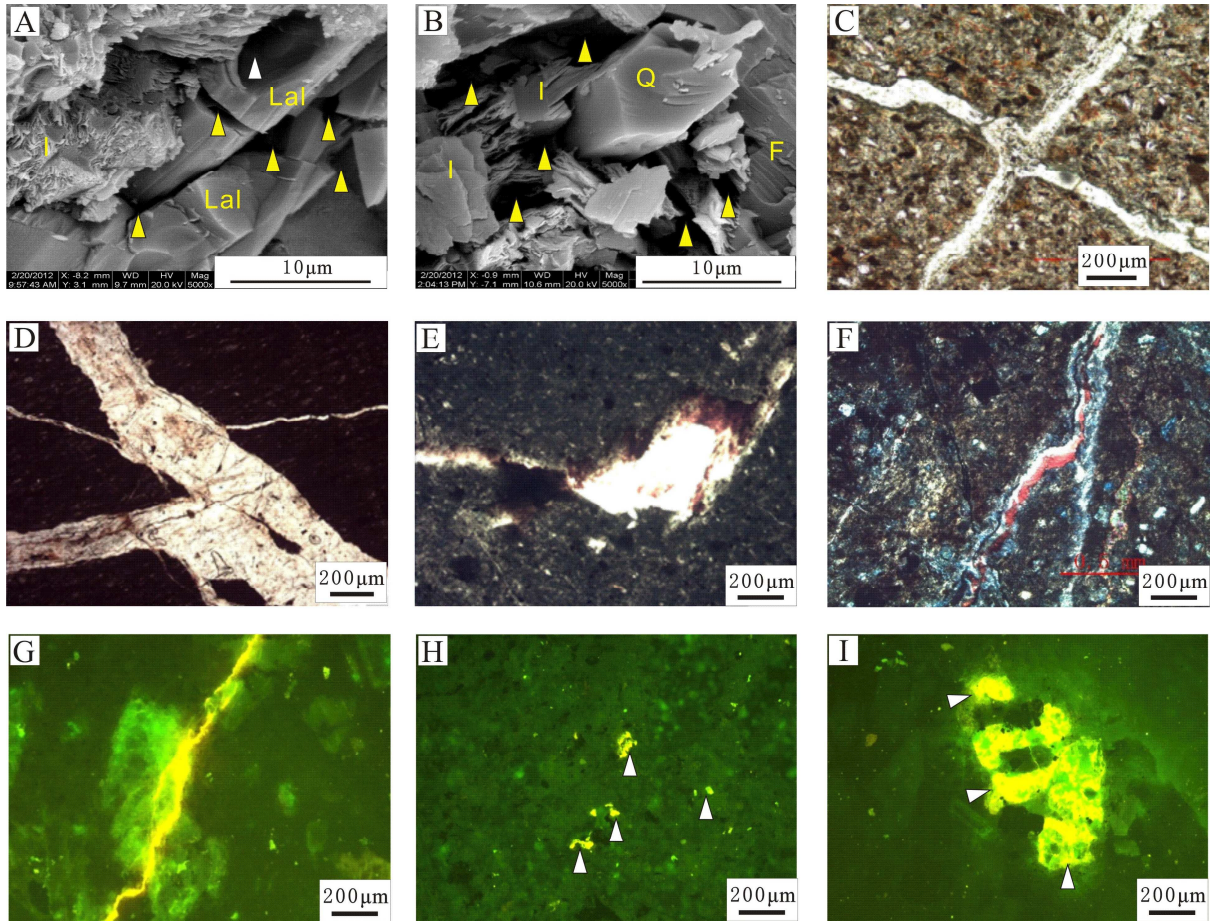


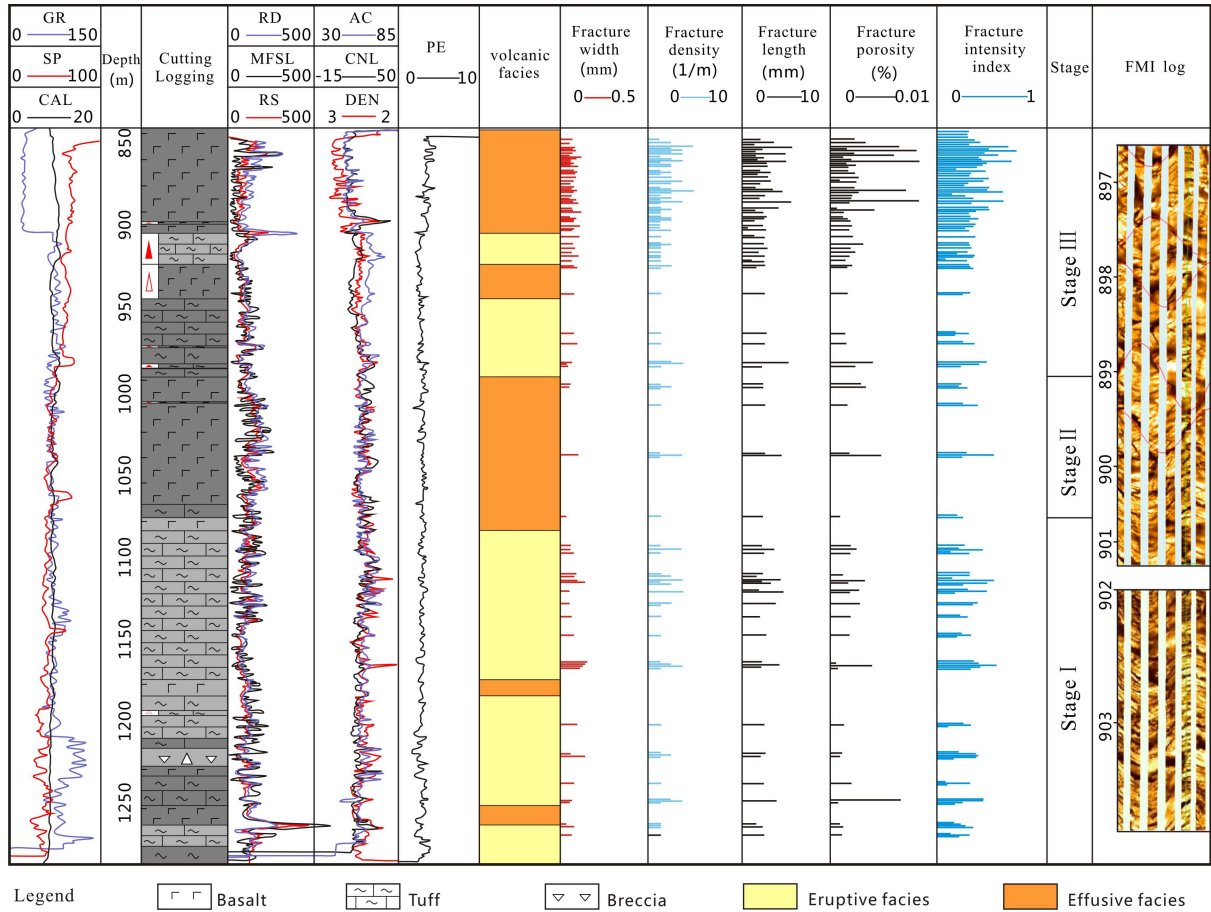


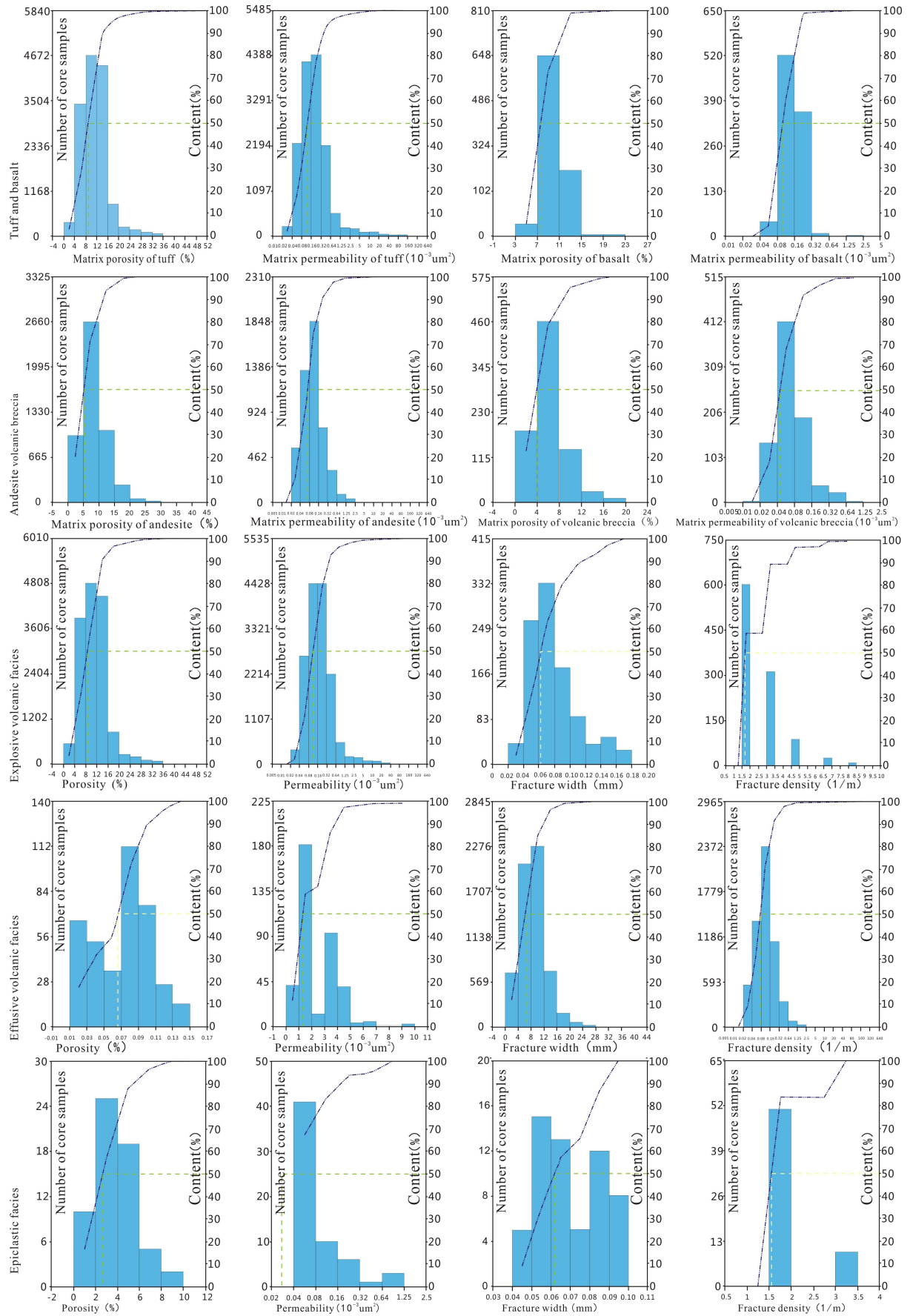


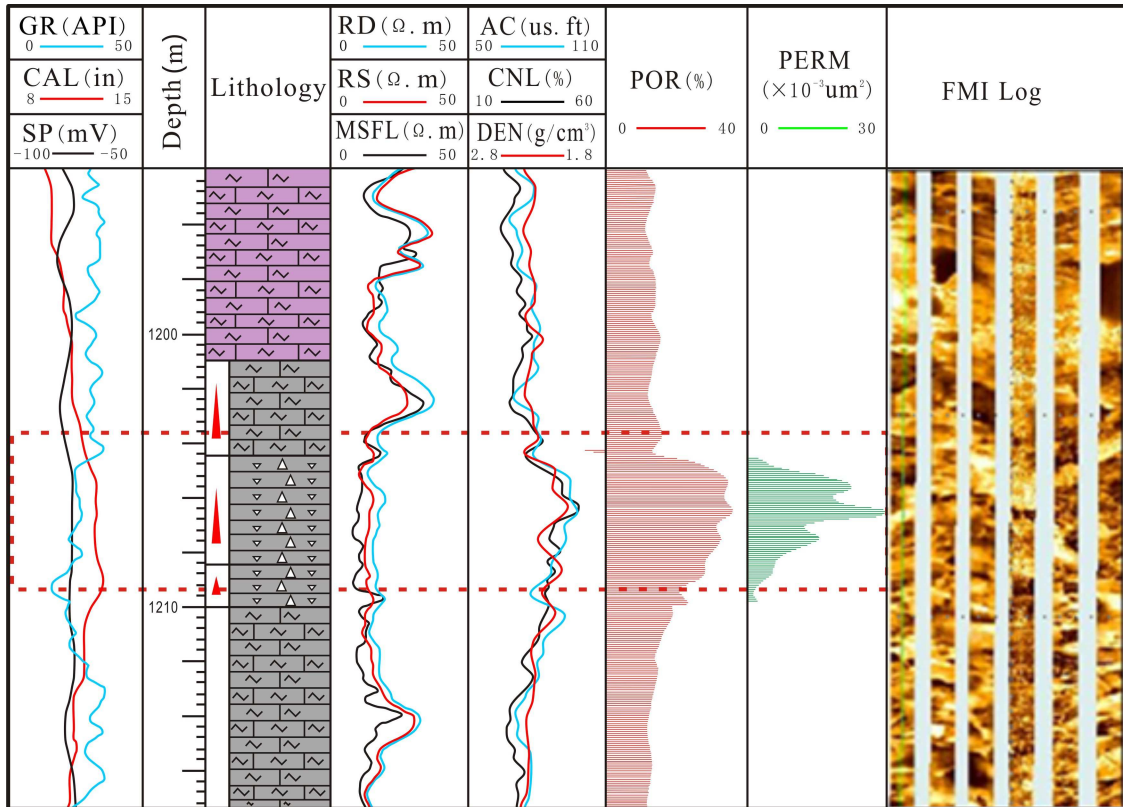


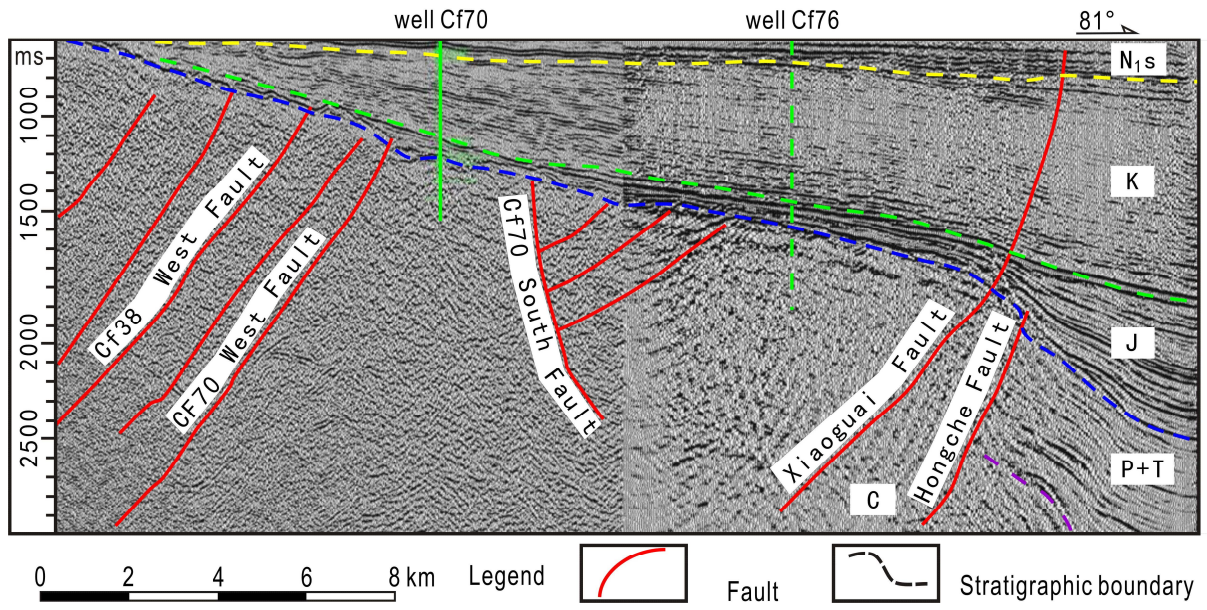


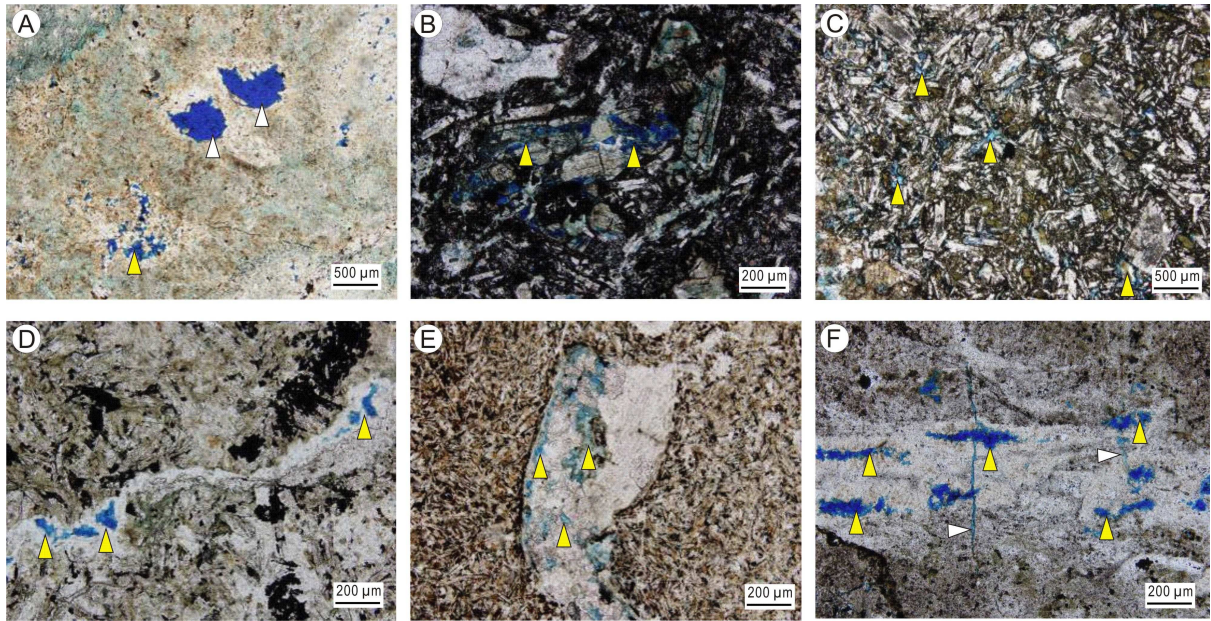


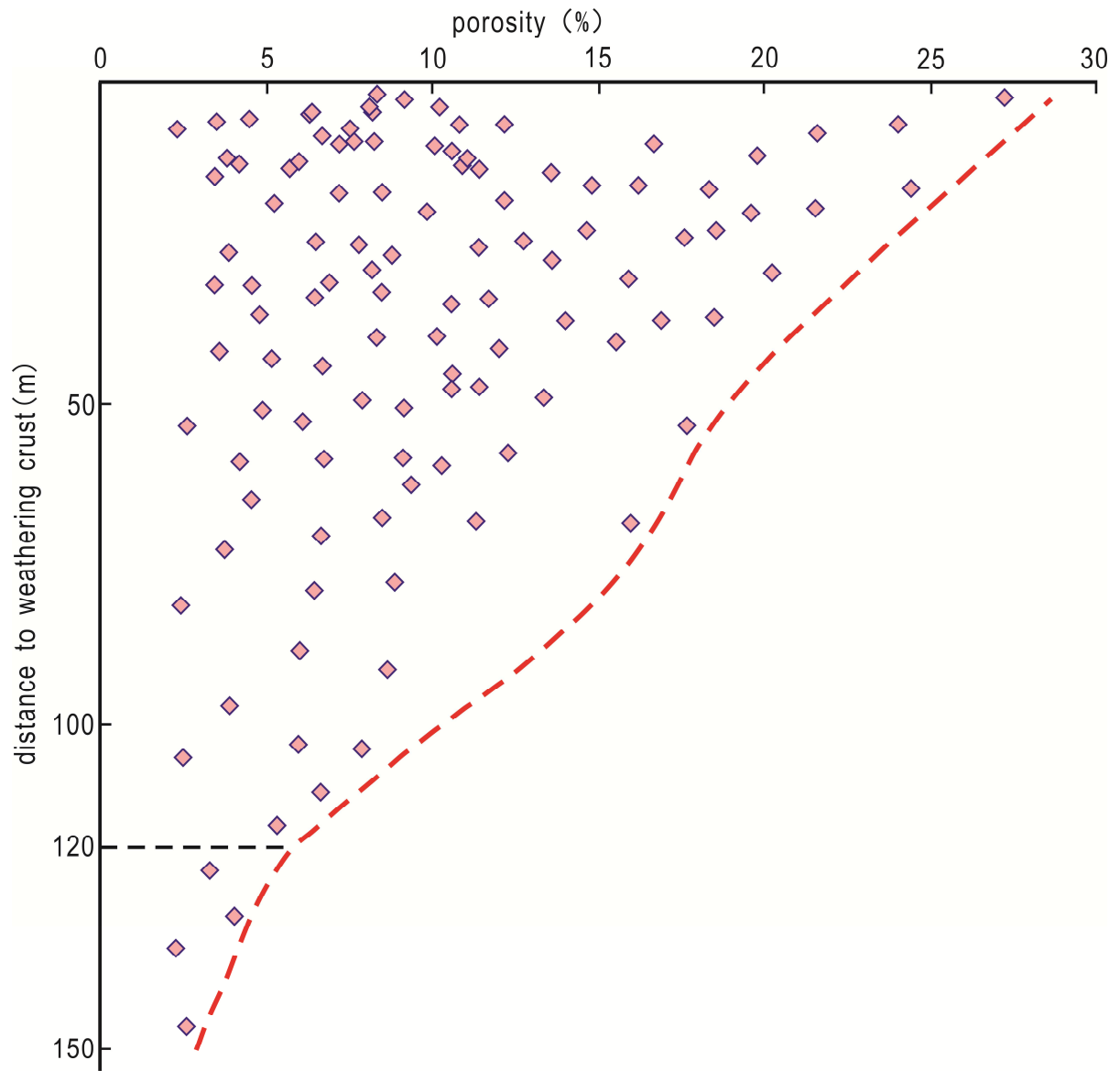


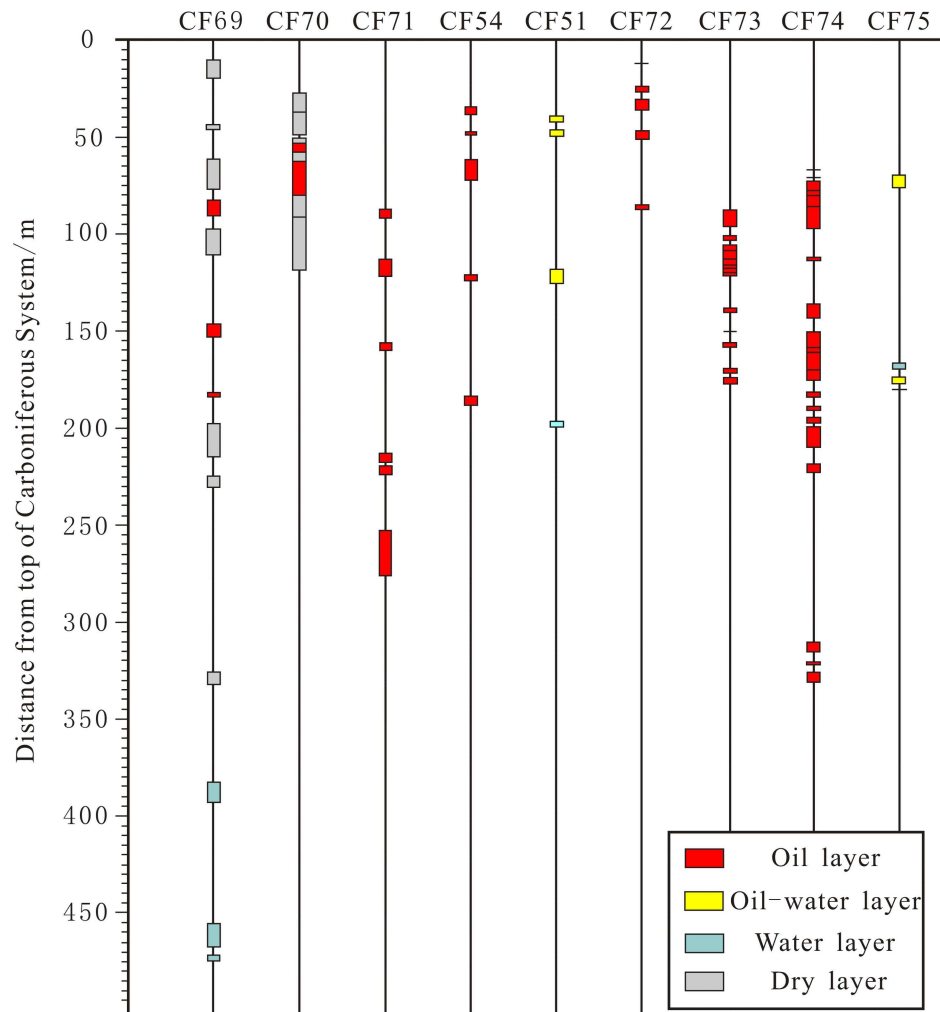


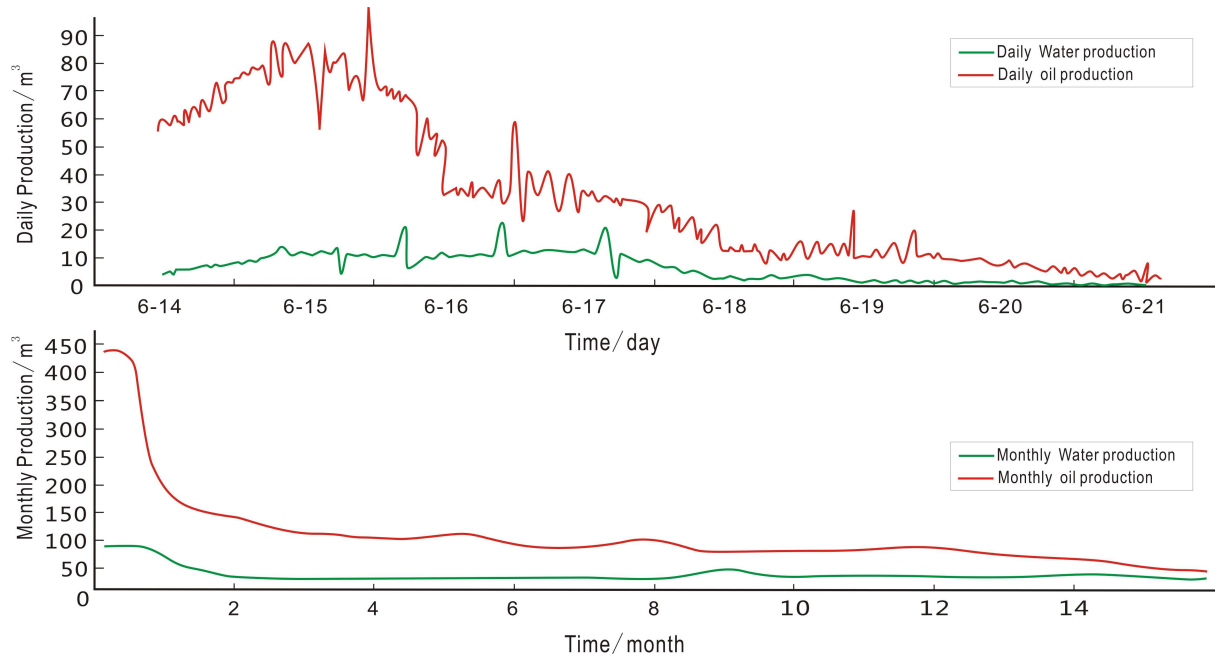


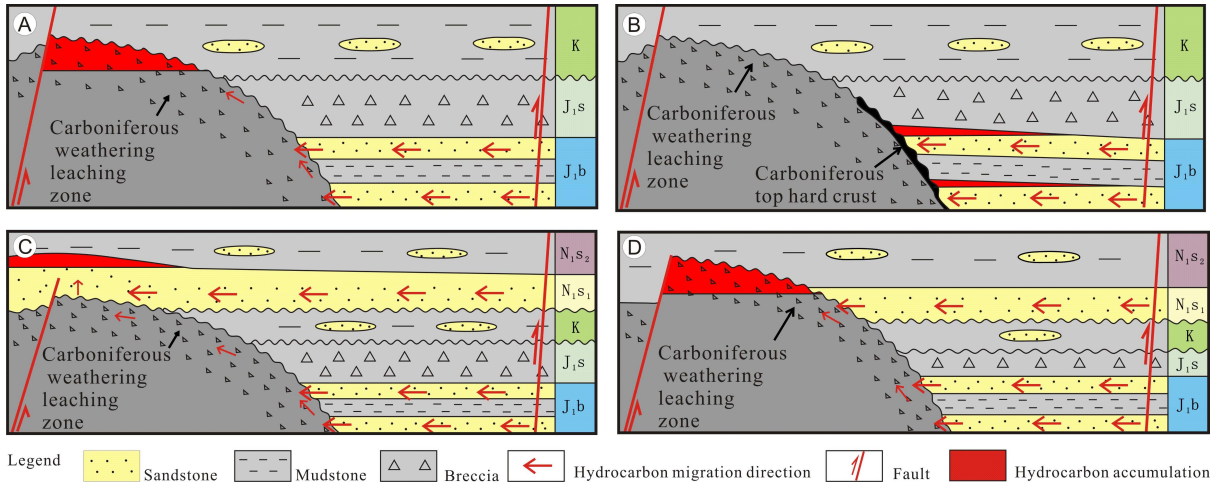












Highlights

- ◆ Tuff and andesitic lava lithofacies exhibit the highest reservoir potential.
- ◆ Tectonic and diagenetic controls on the quality of the volcanic rock reservoirs.
- ◆ Two possible geological models of petroleum accumulation in volcanic rock reservoirs.